3-1999

Space Charge Structure of a Glow Discharge in the Presence of a Longitudinal Inhomogeneity

Frank A. Tersigni

SPACE CHARGE STRUCTURE OF A GLOW
DISCHARGE IN THE PRESENCE OF A
LONGITUDINAL INHOMOGENEITY

THESIS

Frank A. Tersigni, 1st Lieutenant, USAF
AFIT/GAP/ENP/99M-14

DEPARTMENT OF THE AIR FORCE
AIR UNIVERSITY
AIR FORCE INSTITUTE OF TECHNOLOGY

Wright-Patterson Air Force Base, Ohio

The views expressed in this thesis are those of the author and do not reflect the official policy or position of the Department of Defense or the United States Government.

AFIT/GAP/ENP/99M-14

Space Charge Structure of a Glow Discharge

in the Presence of a

Longitudinal Inhomogeneity

THESIS

Presented to the Faculty of the School of Engineering

of the Air Force Institute of Technology

Air University

In Partial Fulfillment of the

Requirements for the Degree of

Master of Science

Frank A. Tersigni, B.S.

First Lieutenant

March 1999
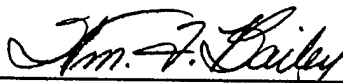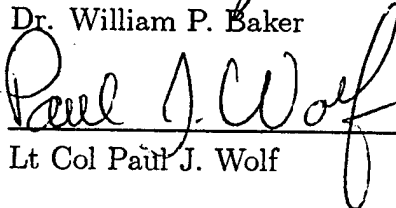
Space Charge Structure of a Glow Discharge

in the Presence of a

Longitudinal Inhomogeneity

Frank A. Tersigni, B.S.

First Lieutenant

Approved:

Wm. F. Bailey _____   _3 March 99_ _____

Dr. William F. Bailey   Date

Chairman

Will. P. Baker _____   _3 Mar 99_ _____

Dr. William P. Baker   Date

Paul J. Wolf _____   _3 MAR 99_ _____

Lt Col Paul J. Wolf   Date

Preface

This thesis is a product of the sacrifice, perseverance and confidence of many people. I'd like to express my thanks first to our Air Force: it's simply an honor to serve in defense of the finest way of life on earth. As for some of my classmates, I appreciate the insightful discussions and shared knowledge offered by Capt Shannon Walker who always entertained any questions I had with much patience. I'd also like to thank Capt Chris Smithtro for various computer tips and his willingness to share the tricky derivations with those tricked. Of course, Capt Kelly Law deserves honorable mention: she simply mixes spunk, perseverance, and (occasional) light-hearted melancholy to a high art form. A hearty thanks also goes out to John MacKendrick at MacKichan Software, who was tireless in his efforts to adapt the AFIT LaTeX style files for Scientific Workplace. Even more tireless was my advisor, Dr. William F. Bailey (AFIT/ENP), whose dedicated professorship prepared many of us for our research and much more. In addition, his commitment to students was always obvious in sacrifices he made for many of us. However, his great skill in guiding students via well placed questions, timely ideas, and consistent encouragement is subtle and only realized by those fortunate enough to have had the experience–and I am thankful for that guidance. Of course, I have to offer a sincere thanks to my children who have endured great sacrifices of family time that they rightfully will get back. Finally, even though she always humbly declines any recognition, my wife is the reason for all of the best things in my life and this document is just as much her accomplishment as it is mine.

<div align="right">Frank A. Tersigni</div>

Table of Contents

List of Figures

Abstract

A survey of space charge structures arising due to inhomogeneities in glow discharges was conducted. Space charge structures associated with tube geometries, the cathode sheath, striations, and shockwaves were examined. Space charge effects on the Electron Energy Distribution Function (EEDF) were explored for a geometric inhomogeneity using an approximate nonlocal solution to the one dimensional Boltzmann equation after Godyak (19). The approximate solution partially captured qualitative aspects of space charge effects on the EEDF. Simplification of collisional effects and adaptation of an approximate electric field restricted quantitative comparisons with experimental data. It is recommended that any future analysis of space charge effects on the EEDF should include energy losses due to elastic collisions, electron-electron collisions and a two dimensional representation of the electric field.

Space Charge Structure of a Glow Discharge

in the Presence of a

Longitudinal Inhomogeneity

I. Introduction

1.1 Objective

The purpose of this study is to survey the space charge structure arising from various inhomogeneities and characterize the nonlocal behavior of the Electron Energy Distribution Function (EEDF) due to an orifice on the axis of a glow discharge. The focus will be to discuss, implement, modify and evaluate an approximate nonlocal solution to the one dimensional Boltzmann equation after Godyak (19).

1.2 Motivation

1.2.1 Anomalous Shock Behavior.   Over the past twenty years, there has been significant interest in the behavior of shock waves in weakly ionized gases. The original Russian investigations due to Mishin et al. [(30), (25), (26)] revealed decreases in shock wave amplitude when propagating through an ionized medium. Further studies since the 1980s, mostly by Russian researchers, revealed similar results and led to additional observations [(3), (4), (5), (6), (7), (10), (20)].

These experiments and further work constituted the emergence of a new discipline, plasma aerodynamics, with the hope of exploiting the observed effects for new aircraft concepts. One such concept, penned AJAX, consisted of an aircraft enveloped in a nonequilibrium plasma enabling long range travel at hypersonic speeds with a reduced effective Mach number. Recently, work in the United States and

1

Great Britain has been accelerated under both governmental and commercial over-sight, respectively. Extensive experimental work continues to be carried on at the Air Force Research Lab [(15),(16),(17)] and also at labs of British Aerospace Corporation based in Great Britain (23).

1.2.2 Space Charge Effects. While observation of the anomalous shock behavior has been extensively pursued, a unified theoretical basis for what is observed remains to be offered. One possible explanation being developed recently includes the formation of a space charge double layer resulting from the faster diffusion of electrons versus positive ions across the shockfront as depicted in Figure 1. The
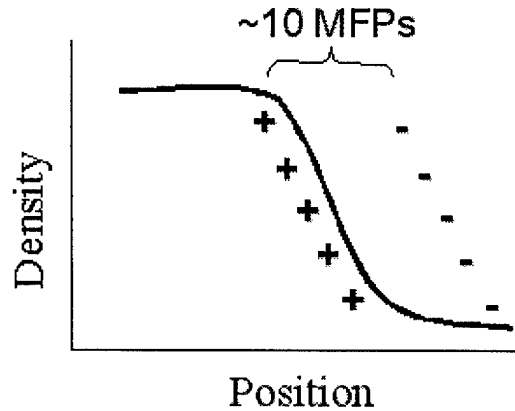
Figure 1   Space charge double layer at shockfront. Space charge region extent is about 10 collisional mean free paths (MFPs) while neutral shockfront width is about 1 MFP.

space charge electric field in the shock frame constitutes a new contribution to the force balance. Notably, this region of charge separation exists on a spatial scale approximately one order of magnitude larger than the neutral shock width.

For the plasmas being considered, the electron energy relaxation length is larger than the distance of charge separation and so the space charge region is a nonlocal, nonequilibrium interface. The possible influence of this space charge region on shock structure and dynamics has been the subject of much debate [(1),(34)]. The

measurement of the electrical properties of this transient phenomenon presents a major diagnostic challenge.

The thrust of the present research is to survey a variety of space charge structures arising in the plasma of a glow discharge. While the causal factors may be different for each mechanism, the symptom is the same: a space charge sheath is formed which requires the problem to be studied in a nonequilibrium, nonlocal fashion where electron momentum transfer and energy relaxation occur at different rates and on different spatial scales. Each volume element of the discharge is not necessarily in local thermodynamic equilibrium. For electrons, which carry most of the current due to their higher mobility, the energy input due to the local electric field is not necessarily balanced by collisional energy losses. Accordingly, a nonlocal treatment is required when the electron energy relaxation length is greater than the applicable scale length for the plasma structure under study.

1.3 Scope

The discharges to be studied will be Direct Current (DC), low pressure (.001-30 Torr) and diffusion will be the dominant charged particle loss process. In general, the plasma will be weakly ionized with fractional ionization, n_e/N, to be less than 10^{-4}. Space charge structures to be surveyed will include stationary (geometric, cathode sheath and standing striations) as well as dynamic (moving striations, shockwaves in plasma) phenomena. The case of an orifice on the axis of the discharge will be investigated in detail using an approximate nonlocal solution to the one dimensional Boltzmann equation after Godyak (19).

The geometric inhomogeneities examined in the positive column of the glow discharge will include a discharge tube of sharply varying radius (constriction) and a tube effectively divided in half such that the intermediate plasma flow is through a small hole (orifice). The cathode dark space (CDS) and negative glow (NG) region of the discharge will also be surveyed where the acceleration of electrons in the CDS

3

and the inelastic processes that dominate the NG are of interest here. Striations (alternating bright and dark bands) occurring in the positive column will also be introduced with an emphasis upon the periodic perturbations in electron number density and ionization rate. The survey of the space charge structure of a shockwave moving through plasma will be based mostly on the analysis of the electric double layer by Hilbun (21).

1.4 Approach

The initial approach to the present problem will be to survey space charge structures associated with various stationary and dynamic phenomena. The space charge structures of the phenomena of interest are depicted in Figure 2.
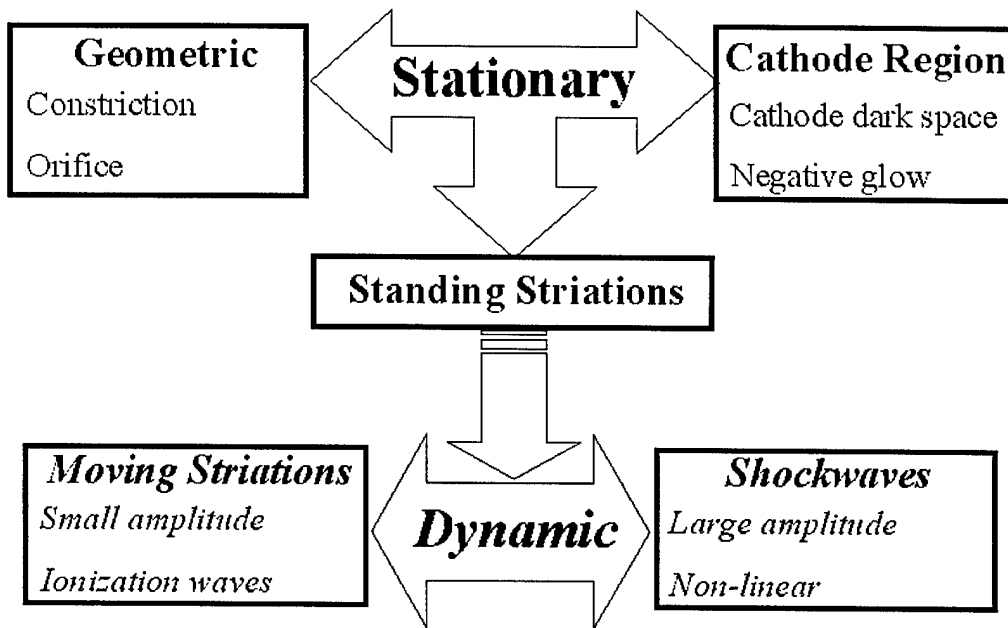
Figure 2   Space charge structures to be surveyed

In each of the cases shown in Figure 2, the space charge structure and associated electric field is a symptom of some kind of inhomogeneity. A fundamental feature among all the phenomena is the requirement of current continuity–the plasma analog

of the mass continuity requirement for an incompressible fluid flowing through a tube.

The analysis of the space charge structures already mentioned will begin with a general survey of some fundamental characteristics and conclude with a more detailed characterization of the nonlocal behavior of the EEDF due to an orifice on the discharge axis. The approach will proceed as follows:

- Survey of space charge structures: stationary phenomena

- Survey of space charge structures: dynamic phenomena

- Analysis of orifice on axis

1.4.1 Survey of Space Charge Structures.

1.4.1.1 Stationary Phenomena.   Beginning with geometric effects, space charge structures will be outlined for a constricted tube as well as a tube with an orifice on the axis. In each case, the normally homogeneous axial characteristics of the positive column are altered as the plasma accommodates the constant current requirement in a tube with rapidly varying cross section. Space charge and associated variations in electric field and potential give rise to an inhomogeneous region where nonlocal phenomena control discharge kinetics. Similarities arise in the analysis of the geometric cases that may be characterized by viewing each as having two distinct sections: a pre-inhomogeneity (potential step) region and a post-inhomogeneity (energy relaxation) region. Experimental results and theoretical approaches to represent the observations will be discussed.

Outside the positive column, maintenance of the self-sustaining discharge will be considered in terms of the cathode (negative polarity) region. Kinetic phenomena in the CDS (also called the cathode fall or Crooke's dark space) region will be related to those in the geometric pre-inhomogeneity region and the negative glow region will be related to the post-inhomogeneity region. The CDS serves as an acceleration

5

region for electrons moving toward the anode (positive polarity electrode). When sufficient energy is gained by the electrons across this potential step, the onset of inelastic collisions (and resulting energy relaxation) serves to mark the extent of the negative glow which is the result of the numerous excitations.

The occurrence of standing striations in the positive column plasma will then be addressed. While the positive column is usually treated as a region of the discharge free of any axial space charge, careful observation under some conditions sometimes reveals periodic perturbations in the charge density manifested as periodic bright and dark bands [(18), (14),(37:293)]. The space charge structure across one spatial period will be compared to the other stationary structures with emphasis on the characteristic distances: the darker zone as an electron acceleration region and the brighter zone as an energy relaxation region.

1.4.1.2 Dynamic Phenomena. Moving disturbances will then be considered beginning with a look at characteristics of small amplitude ionization waves such as moving striations. The moving variety of striations are characterized phenomenologically in a similar fashion to the stationary variety except for their axial motion along the discharge.

Large amplitude waves, such as shockwaves in plasmas, will be addressed with the analytic and numerical results of Hilbun (21). They will be explored with an emphasis on the characterization of the space charge region at the shockfront. Some of Hilbun's results will be compared to the aforementioned space charge phenomena.

1.4.2 Analysis of Orifice on Axis. In Chapter three, focus will be brought upon the stationary geometric case of an orifice on the axis of the discharge. The measurements of Godyak (19) will first be examined with emphasis on the spatial evolution of the EEDF along the discharge tube axis. Then, his nonlocal approximate solution to the one dimensional Boltzmann equation will be discussed and implemented. Results will be examined and modifications to the approach con-

sidered. An evaluation of the approximate solution will be made regarding its applicability as a tool for parameterizing space charge effects on the EEDF.

II. Survey of Space Charge Structures

2.1 Introduction

This study will draw from similar physical concepts as pursued in different analytical settings. Experimental results as well as some theory of stationary and dynamic phenomena will include an introductory discussion regarding glow discharges, discharge tube geometries, the cathode dark space and negative glow, striations, and shock waves. A more rigorous treatment of the geometric case of an orifice on axis will follow in Chapter 3, but for now the emphasis will shift to a survey of these topics, beginning with a brief overview of a typical glow discharge configuration as presented in Figure 3.

2.2 Typical Glow Discharge Configuration

Ordinarily, the experimental configurations enabling measurements of sheath phenomena are conducted under similar operating conditions. A typical DC glow discharge circuit and schematic representation of the observed parameters is represented in Figure 3. Usually, the positive column occupies a majority of the discharge but the other regions are exaggerated in this figure such that they are easily distinguished. The sketched parameters represent values along the axis of the discharge.

Much research has been conducted on the tube of uniform cross section. The typical glow discharge is primarily maintained by positive ion bombardment of the cathode resulting in electron emission from the metal surface. These low-energy electrons eventually travel through the cathode dark space where they gain energy. Once reaching the threshold excitation energy, these electrons undergo numerous inelastic collisions which produces the negative glow. The Faraday dark space is then the transition zone between the cathode region of the discharge (where the electron axial drift velocity is generally large compared to the random velocity) and

8
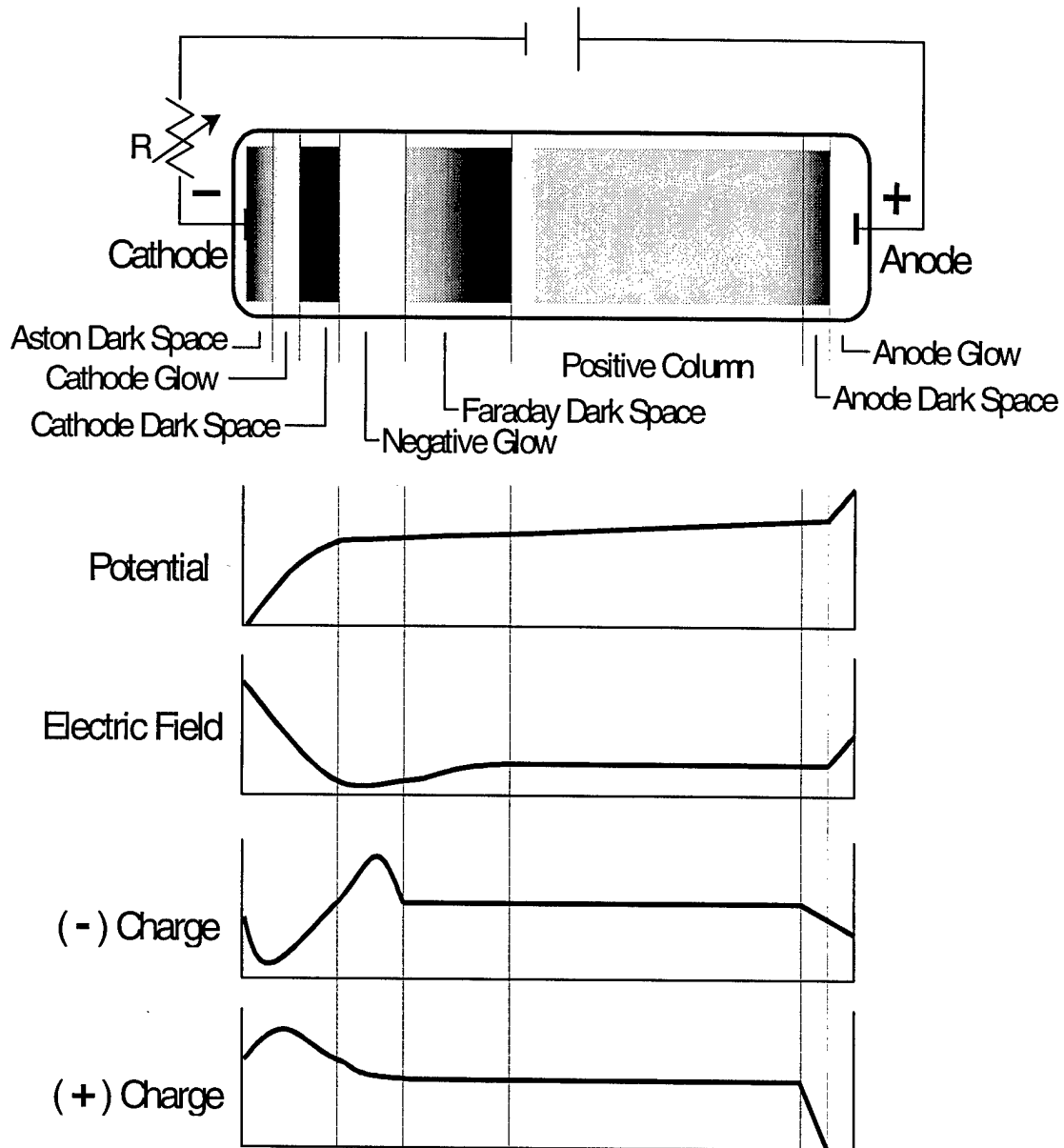
Figure 3   Schematic of D.C. glow discharge. Plotted parameters are axial values and the discharge electric field is from anode to cathode.

the positive column (where the electron axial drift is small compared to the random motions).

Not surprisingly, the most extensively studied feature of the glow discharge is the positive column due to its azimuthal and axial symmetry. Note the constant axial electric field and corresponding lack of space charge along the positive column. The ionization in this region is balanced by diffusive losses to the tube walls along the radial direction (n_e at the walls ≈ 0). Common discharges have radii between 1-5 cm, support currents about 10^{-3} to 1 Amp, electron temperatures of a few eV, and are usually studied at pressures from 0.1 to 1 Torr.

Now, space charge structures associated with some stationary and dynamic phenomena will be introduced beginning with geometric variations of the cylindrical positive column.

2.3 Stationary Phenomena

2.3.1 Geometries.
Two specific geometries causing the positive column to be inhomogeneous are presented here: a constricted tube and an orifice on axis (see Figure 4). The inhomogeneity referred to in this context is that of a longitudinal
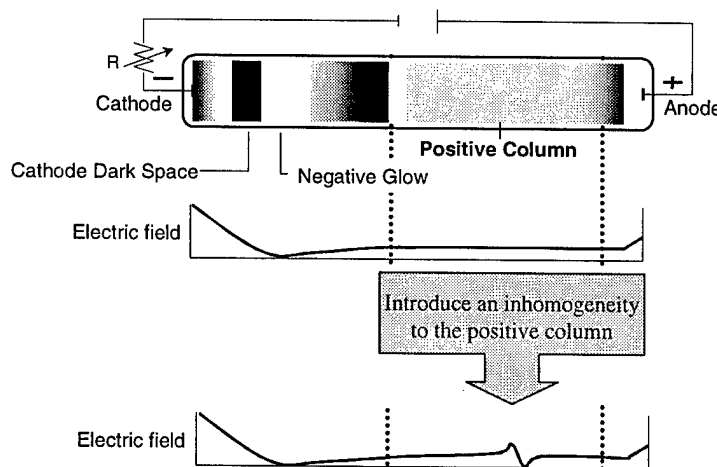
Figure 4   Space charge field resulting from introduction of inhomogeneity to the positive column.

nature, i.e., along the cylindrical axis. The introduction of some form of geometric inhomogeneity results in a perturbation of the otherwise constant axial electric field; a space charge field arises. This is a consequence of the requirement for continuity of the current to be maintained across the change in geometry. The constricted tube case will now be reviewed.

2.3.1.1 Constricted Tube. The tube geometry most often referred to when speaking of constrictions is shown in Figure 5. The double layer potential
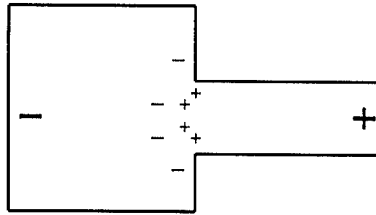
Figure 5   Constricted tube geometry with space charge sheath indicated.

sheath that forms in this case occurs on the cathode side of the constriction (within the larger radius) and measurements for mercury-rare gas mixtures as well as pure rare gas discharges have been carried out by various workers [(2),(11),(12),(35),(36)]. A graphical interpretation of this plasma response as a result of continuity of current is shown in Figure 6 for the case of a tube constriction.

The plasma adjusts by increasing the electron current density to account for the decreased cross sectional area. This is usually observed as an increase in both the electron number density and the drift velocity such that the product of the two quantities accounts for the decreased area.

Note that while the discharge electric field is directed from anode to cathode, the space charge field is directed toward the cathode on the cathode side of the constriction, but toward the anode on the anode side of the constriction. This may be explained by considering the electron number density and temperature are highest near the constriction. As a result, the electron pressure gradient is directed toward the constriction from either side with the resulting electron pressure gradient

$$\int J\, dA = \text{constant}$$

$$J_1 = n_{e1}\, e\, v_{d1}$$

Electrons
from
cathode

$$J_2 = n_{e2}\, e\, v_{d2}$$

E_{axis}

Axial distance
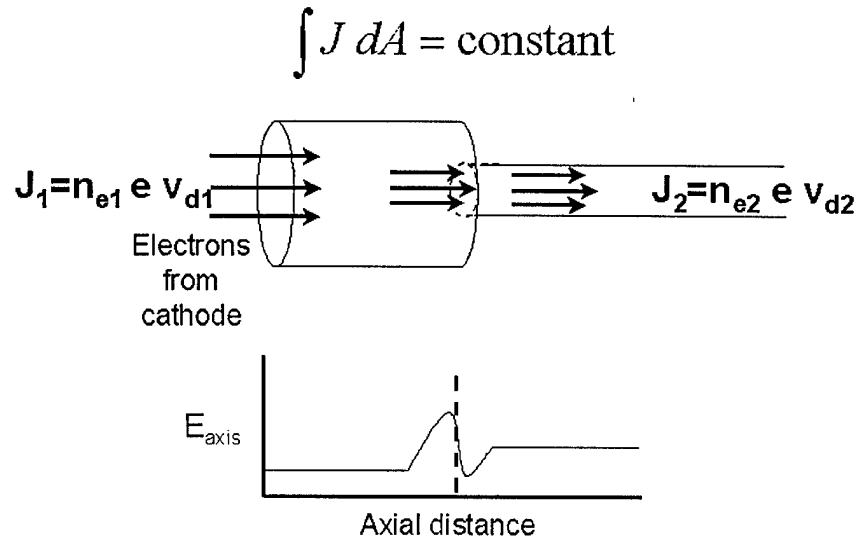
Figure 6   A graphical interpretation of the conservation of current through a constricted tube geometry with cathode on wide side and anode on narrow side. J is the electron current density, n_e the electron number density, e the electronic charge, v_d the electron drift velocity, and E_{axis} the axial electric field directed from right to left.

force per unit charge (i.e., space charge electric field) directed oppositely. So, the superposition of the discharge electric field and space charge electric field results in a total axial field, E_{axis}, that is enhanced on the cathode side and reduced on the anode side.

In 1963, Crawford and Freeston (11) studied a mercury discharge at a pressure of 1 mTorr with currents from 10-100 mA. Measurements of the electron velocity distribution function showed a "double hump" structure close to the constriction. The spatial extent of the bimodal structure was within about 1 cm of the constriction on the cathode side and about 20 cm on the anode side for a wide tube to narrow tube diameter ratio of about 3.3. It was visually noted that the sheath forming at the constriction was approximately hemispherical in shape.

Further studies of the constriction sheath phenomenon came in later years. Andersson (2), about 13 years later, also made measurements of a dual peaked EEDF in front of (pre-constriction, cathode side) and behind (post constriction,

anode side) a stationary plasma sheath. The currents used were two or three orders of magnitude higher than that used by Crawford and Freeston while maintaining approximately the same tube diameter ratio and comparable gas pressures.

A more recent investigation was performed by Sirghi, et al. (36). The experiment was for a helium positive column at pressures around 1 Torr for a wide tube to narrow tube diameter ratio of approximately two. Axial variations of potential, electric field, electron number density, average electron energy, and current densities (diffusion and conduction) are shown in Figure 7.

The electric field shown in panel (a) of Figure 7 is increased just prior to the constriction and reduced just after. This is a consequence of the requirement that the total current through the circuit be maintained as mentioned previously.

A common feature evident in all the cases reviewed for this study is that the electron number density and mean energy peaks are not coincident; the mean energy peaks just prior to the constriction while the electron number density peak is just after the constriction as in panel (b) of Figure 7. While the peak in mean energy may be expected to occur at the constriction after an electron has accelerated through the entire sheath, the pre-constriction peak can be addressed in a physical way using the electron current density measurements found in panel (c) of Figure 7.

Far from the constriction, the diffusion component of the axial current density is small since its magnitude is proportional to the axial electron pressure gradient as discussed before. Close to the constriction, however, the diffusive component is large and directed toward the cathode. This amounts to a diffusive backflux of electrons toward the wide part of the tube due to the increased electron concentration just after the constriction on the anode side. The increased electron concentration there is presumably due to increased ionization by higher energy electrons that have been accelerated through the space charge electric field in front of the constriction (the "fast" group of the aforementioned bimodal EEDFs). This fast electron group can be characterized in the following way. The higher energy electrons lose a large

13
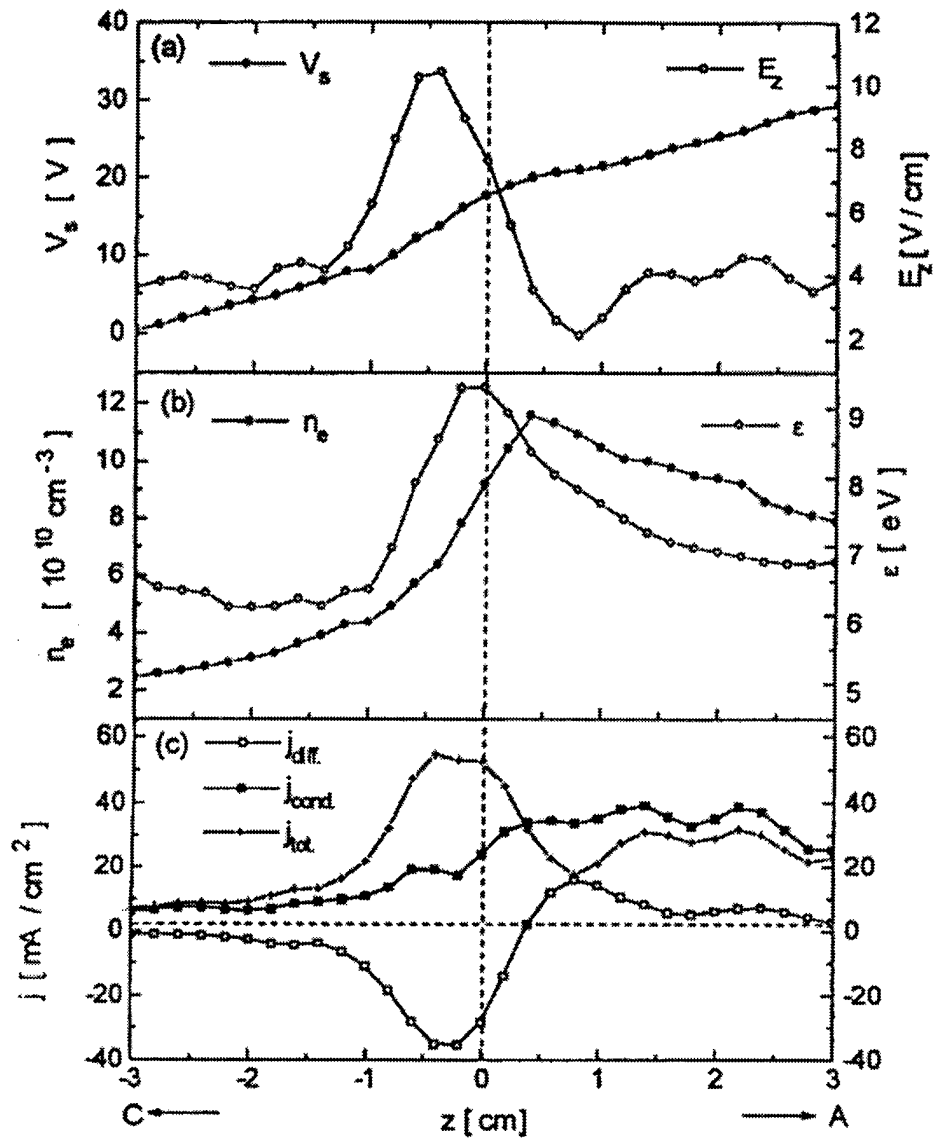
Figure 7   Plotted variables from left to right:
(a) Potential, axial electric field
(b) electron number density, mean electron energy
(c) electron current density (diffusion, conduction, total)
for helium constricted positive column, p=1.4 Torr, I=150 mA.
(After Sirghi, et al. (36))

portion of their energy once reaching the other side of the constriction due to inelastic collisions upon traversing the space charge sheath. They, as well as the progeny electrons on the post-constriction side due to this increased ionization, are at reduced energies. Since their directed velocities toward the anode are now reduced, it is most likely to be these lower energy electrons that comprise the diffusive portion of the current density back toward the cathode.

In this way, the mean energy is reduced just prior to the constriction due to the diffusion of these lower energy electrons (whose motion is retarded in the cathode direction by the enhanced electric field) resulting in a mean energy peak that is shifted slightly toward the cathode.

Axial variation of the EEDF is also measured in the same paper as shown in Figure 8 and it reveals a three dimensional perspective not easily envisioned in the prior work.
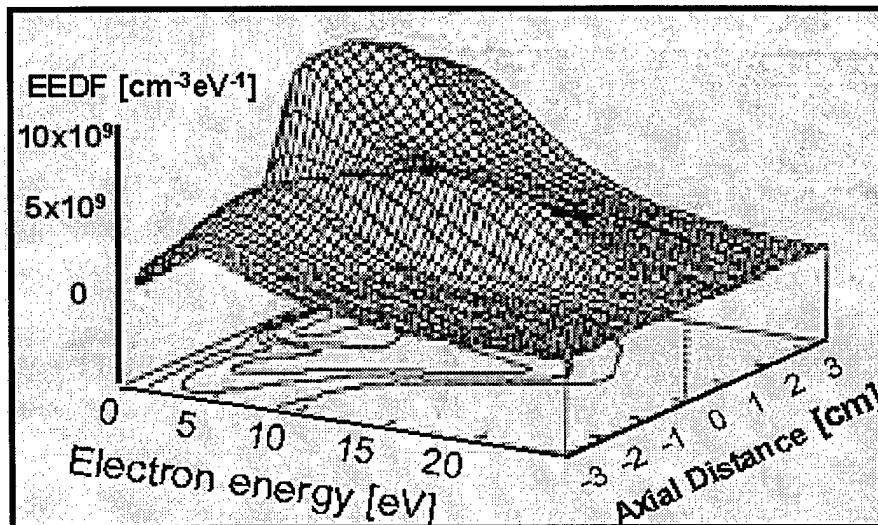
Figure 8   Axial variation of the EEDF for the helium constricted positive column at p=1.4 Torr, I=150 mA. The right axis is distance from the constriction along the axis from the cathode (-3 cm) through the constriction (0 cm) to the anode (3 cm) (after Sirghi, et al. (36)).

15

The EEDF shows the migration of electrons to higher energies upon traversing the sheath with an apparent peak in the average energy just prior to the constriction while the electron number density peak is observed just after the constriction (within 0.5 cm on either side). These results are consistent with the earlier findings due to Crawford and Freeston, and shows almost a six-fold increase in plasma density close to the anode side of the constriction; presumably due to increased ionization by the higher energy group of electrons.

2.3.1.2 Orifice on Tube Axis. Other geometries besides constrictions have also been investigated. Godyak (19) investigated the tube geometry with an orifice on axis. His experimental conditions were similar to previous double layer investigations: Hg-Ne mixture, total neutral pressure about 1 Torr, currents on the order of 0.1 A. The key difference is the orifice on the axis of the tube as opposed to a narrow tube joining the two halves (Figure 9).
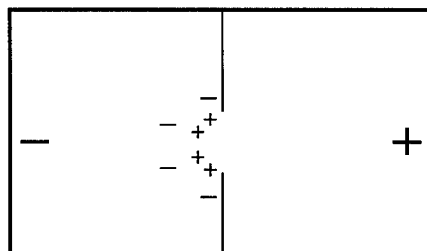
Figure 9   Discharge tube with orifice on axis and space charge sheath.

In this case, the relevant geometric proportionality is the orifice diameter compared to overall discharge tube diameter. Measurements were performed for tube to orifice ratios of two and four with the tube diameter at 5 cm. Measurements of electron number density, mean electron energy, and the EEDF were all performed on axis as a function of distance from the orifice. Similar results were obtained. Mean electron energy peaked at or just before the orifice while the plasma density peaked within 1 cm on the anode side of the orifice (see Figure 10).
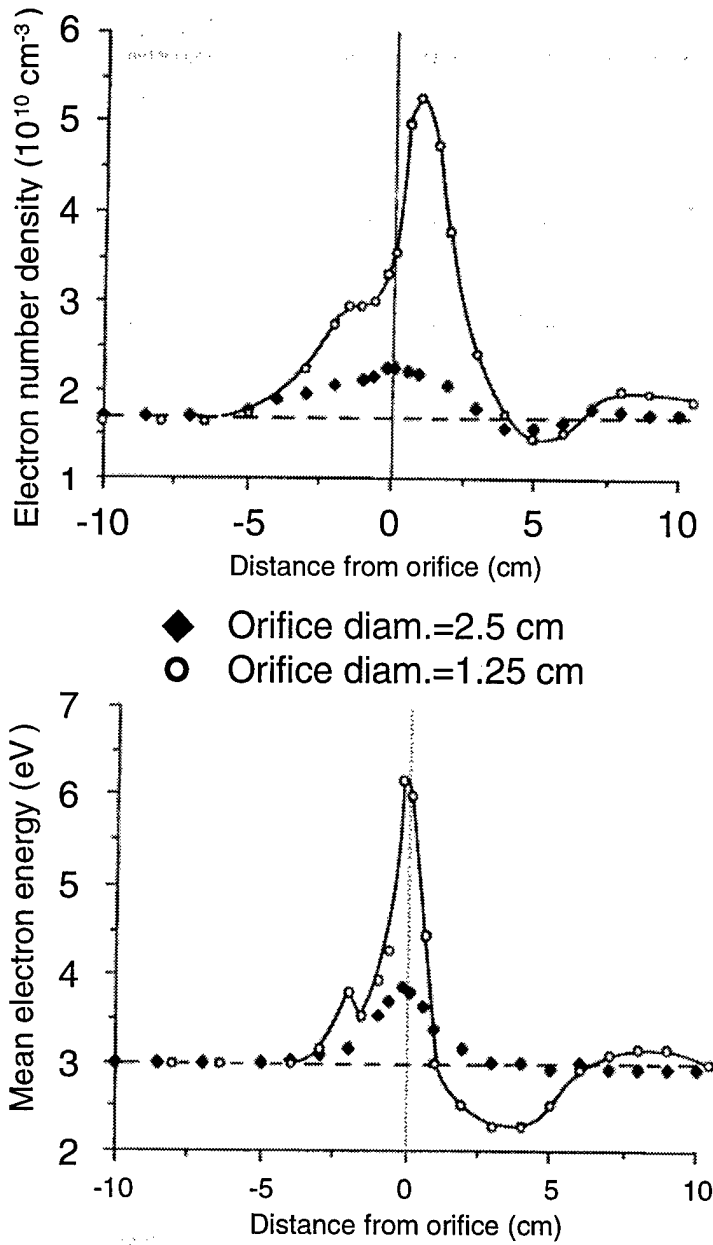
Figure 10   Measurements of axial variation of electron number density and mean energy for orifice on discharge axis, Hg-Ne pressure 1 Torr, current=0.1 A (after Godyak (19)).

Measurements of the EEDF indicated a dual peak structure (Figure 11) within about 0.5 cm pre-orifice (cathode side) and 1 cm post-orifice (anode side).

The forms of the distributions will be thoroughly discussed in Chapter 3, but may be briefly accounted for here. The acceleration of a typical electron moving through the pre-orifice region space charge field occurs quickly enough such that collisional energy losses are small. A typical electron that has not reached the inelastic threshold energy will be predominantly limited to elastic collisions in the region with fractional energy loss per elastic collision proportional to the ratio m_e/M, the ratio of the electron to neutral particle mass. Essentially, the electrons travel through the pre-orifice region and gain energy until the inelastic threshold energy is reached. At that point, a single inelastic collision results in an energy loss of the inelastic threshold energy. So, the pre-orifice region is characterized as an energy gain region and the post-orifice region as one of energy loss. So, there is a migration to higher energies followed by a rapid dumping of the higher energies to lower energies.

Values of potential and electric field were also measured with the increased electric field in the sheath region near the orifice about 5 times the value far from the orifice in the homogeneous region and a decreased electric field (less than the homogeneous field of the unperturbed positive column) present in the post-orifice region.

In addition to the measurements, Godyak also attempted to develop a simplified kinetic equation to capture the spatial evolution of the EEDF near the orifice. This will be pursued in detail in Chapter 3. For now, the discussion will shift away from geometric inhomogeneities and toward the cathode dark space and negative glow.

2.3.2 Cathode Dark Space and Negative Glow. Thus far, the focus has been upon processes predominantly occurring in the positive column plasma of the
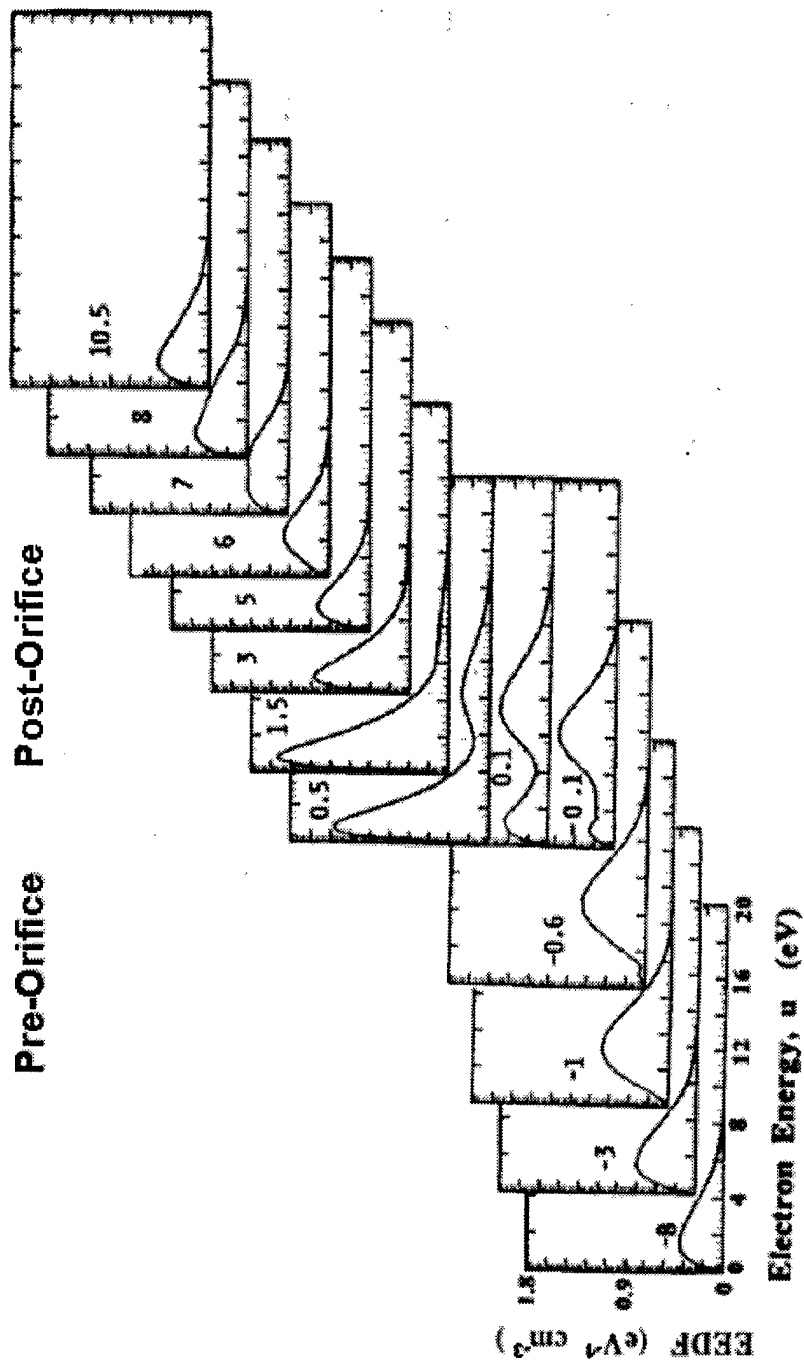
Figure 11   Spatial variation of axial EEDF from cathode to anode with orifice on discharge axis, Hg-Ne at 1 Torr, current=0.1 A. Note the numbers in the upper left of each panel indicate the distance from the orifice in cm, cathode side is pre-orifice, anode side is post-orifice, and the EEDF scale is divided by 10^9 (after Godyak (19)).

19

glow discharge. Attention will now be given to processes in the region near the cathode with the focus here on the cathode dark space and the negative glow. The main characteristics of the region and its applicability to understanding space charge structures in the discharge will be given here.

Recalling the discharge configuration from page 3, the electrodes at either end of the discharge tube permit current to flow between the external voltage source and the plasma within the tube volume. The negatively biased electrode, the cathode, acts as an electron source ultimately maintaining the discharge. While direct emission processes such as electron emission from the cathode due to the metal surface temperature (thermionic) are present, the dominant electron emission at typical operating conditions is due to indirect (also called secondary emission) processes resulting from energetic particle (including photon) bombardment of the cathode surface. In the simplest explanation, positive ions initially produced in the region by any process are accelerated toward the negatively charged cathode. Ions impinging on the surface in this manner will cause further surface emission. Due to the strong potential gradient in the vicinity of the cathode, electrons generally do not have an appreciable flux in its direction.

The electrons generated at the cathode via ion bombardment are initially accelerated through the short length of the Aston dark space, where they do not yet have sufficient energy to excite or ionize the gas. The next region encountered, moving from cathode to anode, is the cathode glow. This is also a region of small axial length and appears at the point along the discharge where excitation due to electron collisions begins to occur (33:130). The next region encountered is the cathode dark space which is characterized by ionization growth due to electrons accelerated through the strong electric field. Two electron energy groups arise. The high energy group are those responsible for the electron multiplication in the region and their energies are high enough such that relatively little excitation occurs. The newly produced electrons in this region are initially at energies generally lower than

the excitation energy threshold so this region is relatively dark. The thickness of this dark space generally corresponds to the distance the lower energy electrons must travel before reaching the inelastic energy threshold. This distance is phenomenologically similar to the pre-constriction (or pre-orifice as the case may be) space charge sheath as given in previous sections.

An average electron, upon reaching the inelastic threshold energy, can undergo an inelastic collision in the negative glow region. Both the low and higher energy groups experience large energy losses in the negative glow due to inelastic processes. The slow group is responsible for the excitation and resulting increased light output in the region, while the fast group can cause ionization but penetrate farther into the negative glow. The light intensity decreases with distance from the cathode according to the distribution of the higher energy electron group, and the transition is finally made to the Faraday dark space and then the positive column as the electron random energy begins to exceed the diminishing directed energy. The negative glow region can be compared to the post-constriction region or post orifice region.

The boundary of the cathode dark space and negative glow can be thought to represent a boundary analogous to the geometric inhomogeneity boundaries. The dominant energy relaxation mechanism (inelastic collisions) and the behavior of the EEDF in each case are in qualitative agreement. While the space charge structure in the cathode region is not associated with the geometry, the applicable physics governing the electrons in the cathode dark space and negative glow are similar to the geometric inhomogeneities considered thus far, albeit at significantly higher values of potential.

2.3.3 Standing Striations. The D.C. discharge apparatus has also been used in many other types of configurations to explore wavelike activity within the plasma such as ion and electron plasma oscillations. The D.C. positive column plasma, in particular, exhibits oscillations of the striation and ion-acoustic types.

Even in steady state conditions, fluctuations in the plasma can be observed as periodic light and dark regions [(14:137),(18), (29),(37:292)]. These striations, as the light intensity variations are referred to, are indications of electron energy and charge density variations. The alternating light and dark bands along the axis of the tube may appear stationary or as moving pulses of light, known as stationary or moving striations, respectively.

A stationary striation wave is usually found to be curved in a convex manner toward the cathode end of the discharge with the brightest portion most well defined on the cathode side and more diffuse on the anode side [(14),(18)]. The peaks of the electron number density coincide with the bright regions of the wave. This modulation in electron density causes a space charge potential to exist between multiple striations, with a magnitude found to be approximately equal to the inelastic energy threshold in many cases. This relation can be recalled to be similar to previous discussions of the cathode fall length as well as the sheath in front of a geometric inhomogeneity. The double layer sheaths at constrictions or other types of boundary phenomena may be thought of as a single stationary striation (see Figure 12).

A striation, then, is perhaps a more general description of the double layer structures discussed thus far.
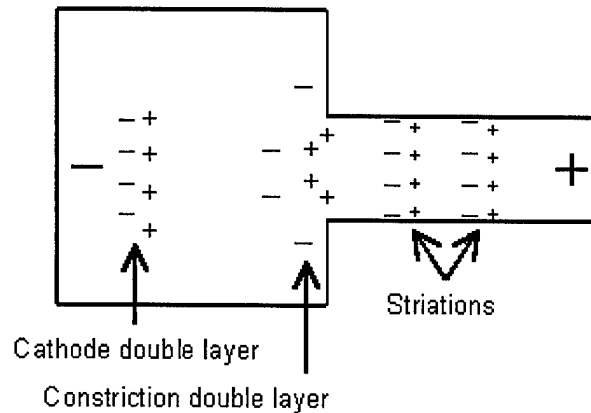
Figure 12   Constricted tube with striations.

The discussion to this point has concentrated on stationary space charge structures in the presence of longitudinal inhomogeneities. Now the review will move on to dynamic phenomena associated with non-stationary space charge structures.

2.4 Dynamic Phenomena

2.4.1 Moving Striations.

These phenomena, like their stationary counterparts, are generally small amplitude instabilities that may occur in the plasma of the positive column. At low gas pressures or pressure-radius product, $pR \lesssim 0.1$ Torr-cm, the wave structure tends to be of the ion-acoustic variety where perturbation of the ion number density occurs with approximately constant phase velocity (18). For higher pressures, striation waves (i.e., ionization waves) are more commonly observed and include perturbation of the electron number density and electron energy where the peaks usually have a constant phase difference.

In cases of moving striations, the peak of the potential variation at the head of the disturbance is approximately equal to the first ionization potential of the gas. They have been found to move toward the cathode as well as toward the anode. Frequencies for moving striations are approximately in the range $10^3 - 10^5$ Hz. A further significant observation of the variations is that the electron energy peak leads the electron number density peak along the axis by a phase difference of approximately $\pi/2$ [(18), (32)]. This is a feature that is analogously consistent with the stationary phenomena measurements of Godyak (19) and Sirghi (36).

Analysis of striations is one example of the advantage of nonlocal methods. As Kolobov and Godyak note (29), the characteristics of these waves revealed by nonlocal kinetics (such as anomalous dispersion) is not predicted by hydrodynamic methods. As in Landau damping where the wave-particle interaction requires a kinetic approach to be modeled physically, the processes of interest here require similar treatment if they are to be fully described.

A result and discussion from a review of nonlocal electron kinetics in 1995 by Kolobov and Godyak (29) will be highlighted here. In many cases, such as the well known phenomena of Landau damping, response of the EEDF to perturbations in potential (or electric field, ionization rate, etc) has been explained with kinetic theory (although in that specific case complex integration, i.e., residue calculus, is employed).

However, for our case, when the spatial period of the electric field is comparable to the excitation energy acquisition length ℓ of an electron in the plasma, self-excited oscillations may occur. For instance, an excitation threshold of 5 volts such as for mercury with a perturbed electric field of 3 volts per centimeter would have an energy acquisition length of $\frac{5}{3}$ or approximately 1.6 centimeters.

If the spatial extent of the electric field perturbation is comparable to this distance, resonant EEDF response to the modulation in electric field may occur. A resonance, or instability, occurs when the parallel phase velocities of the wave and particle are the same. In this way, where for our case a spatially or temporally periodic electric field is parallel to the electron motion, the wave structure and the particle can interact (exchange energy).

This instability has been found to occur under a variety of conditions and even ordinary ion-acoustic waves have been found to undergo growth due to instabilities presented by double layer electric fields (24). The instability arises possibly due to the phase difference between the high energy tail of the distribution and the peak of the electric field perturbation. Hence, an energy gain or loss of the high energy group could take place.

Other work done by Sirghi (36) examined self-excited as well as externally excited ionization waves in a helium positive column geometrically similar to Crawford and Freeston's experiment. The resonant behavior of the EEDF with respect to the perturbation in the electric field affects the wavelength, as well as the phase and group velocities of the wave, with the group velocity directed toward the anode and

24

the phase velocity oppositely directed (for the narrow tube section on anode side). In this way, the electrons streaming from the cathode provide a feedback mechanism between the external circuit and the excited waves (36).

Recalling the EEDF structure in any of the inhomogeneous cases observed so far, Figure 13 seems to be the dynamic analog of the spatial variation of the EEDF associated with a stationary space charge structure. The spatial period of the electric field in the figure is $\ell/0.928$. In the figure, different curves correspond to different positions along the axis of the discharge. It is apparently very similar to the distributions viewed near inhomogeneities thus far in terms of the migration of electron groups to various energies.
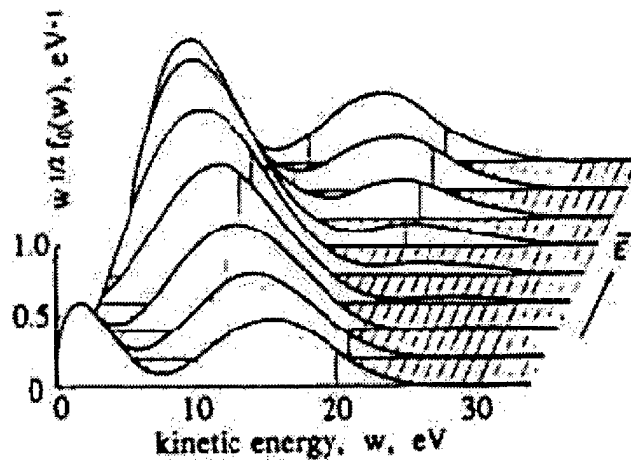
Figure 13   EEDF in a modulated periodic electric field in helium at E/p=12 V/cm/Torr. The different curves correspond to different axial locations along the discharge (after Kolobov and Godyak (29)).

The variation of the EEDF over one period in this dynamic case is phenomenologically similar to what is observed for the stationary cases: migration to higher energies in an accelerating electric field followed by inelastic relaxation. In this case, inelastic relaxation at the bright point of the striation where the electron charge density is peaked.

It is difficult to model such wave-particle interaction using hydrodynamic or any other local approaches. The assumption a local Maxwellian is achieved at each point in space via numerous collisions is central to that kind of development. However, the kinetic behavior of the electrons for these bimodal EEDF structures is not driven by the electrons at the mean energy or some "equivalent" temperature as in a Maxwellian sense. Most of the electrons are either above or below the mean energy, and these two higher and lower energy electron groups are responsible for specific behaviors not able to be captured by localized Maxwellian treatments.

A short review of the anomalous behavior of shock waves in plasma and discussion of the space charge structure as mentioned in the literature will be given next.

2.4.2 Shockwaves in Plasma. There has been a considerable range of physical conditions yielding the anomalous shock behavior in plasma (compared to shock waves in unionized gases) that are cause for research interest. The discharges used have been at pressures of approximately 1-100 Torr, with a range of constituents such as helium, nitrogen, neon, argon, carbon dioxide and air. The discharge plasmas have been weakly ionized with n_e/N less than 10^{-4}. The shock waves have exhibited anomalous behaviors in weakly ionized plasmas compared with neutral gases including (i) shockfront broadening and decreased amplitude, (ii) increased shock standoff distance, (iii) shockfront splitting, and (iv) shock front acceleration [(5), (6),(7),(25),(27),(28),(30)].

These effects also may persist up to approximately hundredths of a second after the external electric field in the discharge is turned off (26). In addition, the shocks have been observed to maintain their anomalous character even in regions without gas heating effects present (28). The flows have generally been at Mach numbers less than five with variations in gas density across the shockfront yielding ratios, $\frac{\rho_2}{\rho_1}$, of approximately three to four where ρ_1 and ρ_2 represent densities upstream and

downstream, respectively. Similarly, gas temperature variations are on the order of 10^2 degrees Kelvin.

Two primary methods for initiating shocks in a discharge plasma are usually employed: the Riemann case and the spark initiated case. The usual Riemann type of configuration is a tube of uniform cross section with two sections of differing characteristics (such as gas density) that are separated by a thin diaphragm. To generate the shock, the diaphragm is ruptured forming what is known as the contact discontinuity, then the interface of the two regions of differing density propagates away from the initial point of contact. The spark initiated shock is generated by imposing a large potential difference across a short gap distance such that breakdown occurs and heats the gas within the gap. This pulse of gas, at high pressure and temperature, then forms the shock.

Contrasted with the stationary small-amplitude space charge phenomena already discussed, measurements of the shockfront have not included EEDF or detailed electrodynamic measurements. Often, bulk density, pressure and temperature variations are the emphasis since measuring microscopic quantities such as the EEDF when the shockwave is moving at hundreds of meters per second through a relatively short length of tube is not a task suited for current Langmuir probe techniques.

For the shockwaves in weakly ionized unmagnetized plasmas being considered, three wave modes may be addressed from the three fluids comprising the plasma: acoustic, ion-acoustic, and electron (plasma) waves corresponding to the neutral, positive ions, and electrons comprising the plasma. Since the space charge region of the shockfront is of interest here, the ion-acoustic wave deserves mention. These are low frequency waves in comparison to electron oscillations, and they have been mentioned in much of the literature as a possible heating source of the neutrals through damping mechanisms at the shockfront (21).

The study of the ionization wave at the shockfront precursor is generally done using fluid dynamic treatments. A conclusion reached by those who have researched

the shock phenomenon is that for the energy densities necessary to alter the characteristics of the acoustic (neutral) wave, the corresponding ionization fraction must be at least three orders of magnitude larger than the degree of ionization in the plasmas under study (21). However, the possibility of a locally higher fractional ionization at the shockfront has not been ruled out by any of the analyses and, in fact, some have claimed evidence exists for this possibility(20).

The work of Hilbun (21) will be used to outline fluid dynamical treatment of the shock characteristics. Here, many of the restrictions of previous linear, time independent developments (3) were removed and a numerical solution to the Euler equations including energy flow terms obtained. The system is modeled as two fluids but nonlinear dependencies are retained and no form is assumed for the neutral density and velocity variation as had previously been done. Further, the electron temperature is assumed to be constant across the shockfront.

This analysis, as the earlier fluid treatments, predicts the formation of a space charge double layer ahead of the neutral shock with an approximate width ξ_o given by $\frac{T_e}{T_n}\lambda_{in}$, where T_e is the electron temperature, T_n is the neutral gas temperature, and λ_{in} is the ion-neutral collisional mean free path in the upstream (undisturbed) flow. Using values similar to the previous steady state analysis yielded comparable results. The region of the space charge potential, sometimes referred to as the precursor region, is estimated to be about an order of magnitude too small for an effect such as increased ionization to be observed at the shockfront. The relations of the potential (Φ), electric field (E), and precursor width (Δx) are reproduced from Hilbun (21) in Figure 14. Note that at these pressures, the peak electric field is nominally an order of magnitude larger than the lower pressure stationary phenomena already reviewed.

He conservatively estimates a nominal ionic energy density capable of affecting the neutral flow that is 1/10 of the neutral energy density. He then estimates a necessary minimum ionization fraction, assuming ion random and flow velocities are
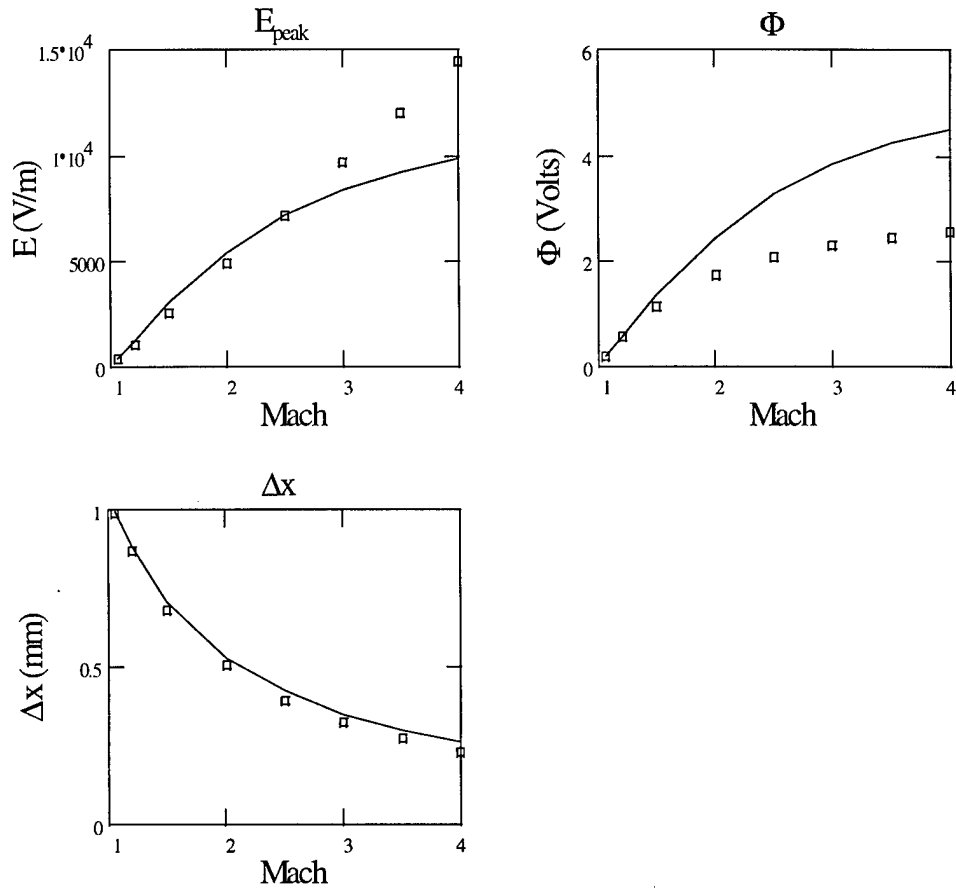
Figure 14   Hilbun's (21) numerical calculations (boxes) and analytic estimates (solid lines) of peak electric field (E), potential (Φ) and precursor width (Δx) versus Mach number.

comparable, for the ions to alter the characteristics of the neutrals This resulting critical fractional ionization is about 10^{-3}, approximately three orders of magnitude larger than what is commonly observed in typical glow discharge plasmas.

This result is somewhat unsatisfying, considering the effects of space charge potentials that have been reviewed. In most every case, the space charge region is accompanied by an associated energy relaxation region, owing to the nonlocality of the problem. The sheath region, in the other cases reviewed here, has dramatic effects upon the EEDF even in the case of moderate perturbations of the potential. The profile of the electric field in the sheath region as calculated by Hilbun is given in Figure 15.
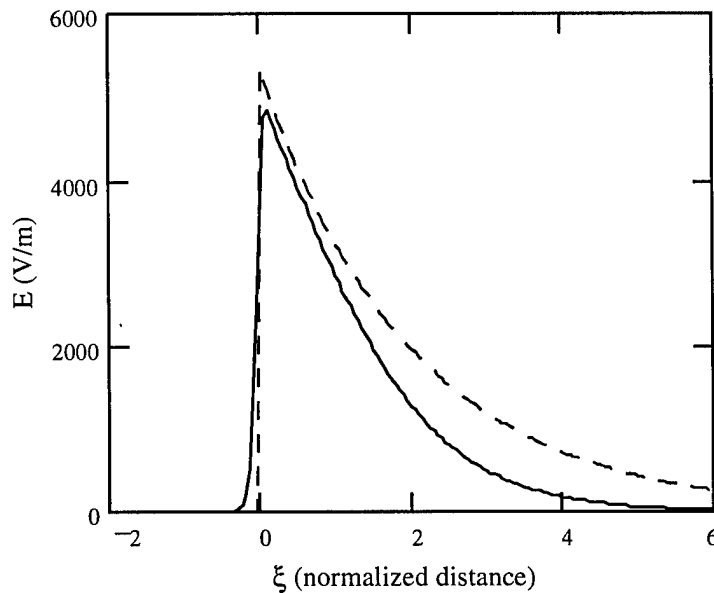
Figure 15   Hilbun's (21) numeric (solid line) and analytic (dashed line) determination of the electric field in the shock front region. The normalized distance, ξ, is the shock distance normalized to the precursor width ξ_o.

Recalling the discussion in the previous section, resonant exchange between wave-particle is a possibility if the precursor width is of the order of $\ell = u_1/E$ where u_1 is the inelastic threshold energy. In the case of a Mach 2 shock in argon at 30 Torr,

a nominal value for ℓ is approximately $\frac{10V}{50V/cm}$ or 0.2 cm. This is about five times larger than the precursor width as calculated using a fluid analysis. However, the space charge region of the shockfront is probably better described using a spatially dependent form for the Boltzmann equation, rather than the collisionally dominated homogeneous form inherent in forming a closed set of velocity moment equations.

Predominantly, the careful numerical work by Hilbun reinforced many aspects of the analytic simplifications carried out by Avramenko (3) and others. Considering the potential structure induced at the shockfront, it seems an approach accounting for spatial variations in the energy distribution would be appropriate for thoroughly investigating the region.

2.5 Discussion

In this chapter, space charge structures associated with various longitudinal inhomogeneities were surveyed. Stationary (geometries, cathode fall, standing striations) as well as dynamic (moving striations, shockwaves) structures were considered. In each case, the plasma accommodates the inhomogeneity such that the total current is constant. The space charge field is a consequence of this plasma response. This characteristic of the plasma can be compared to the case of an incompressible fluid flowing through a tube of changing cross section. In the fluid case for steady state conditions and radially invariant velocity, the volume flow rate of the fluid (velocity times cross sectional area) is a constant. For the plasma also in the steady state and with radially uniform velocity, the volume flow rate of the charged particles (drift velocity times cross sectional area) is a constant. The electrons are doing most of the "flowing" in the form of the current due to their higher mobility as compared with the ions.

The stationary space charge structure is then an appealing starting point for the study of the electron kinetics through the region. In addition, for small amplitude dynamic phenomena, the stationary structures under study may be viewed

as a single spatial period i.e., the stationary space charge sheath versus the striation wave. Large amplitude phenomena were also surveyed in the stationary and dynamic case such as the cathode dark space and negative glow region and the shockwave in plasma, respectively. In all cases the environment under study is not only characterized by some nonequilibrium interface, but also by nonlocality. In the case of the discharge tube, the electrons are moving through the acceleration region (sheath, pre-constriction, pre-orifice, CDS, etc.) in a characteristic time that is much shorter than the characteristic time for them to be lost via some loss process, such as radial diffusion to the tube wall. This is contrasted with the usual conditions of the positive column where axial drift is comparatively slow. Similarly, the acceleration region may also be viewed in terms of the energy gain and loss for an electron moving through it. The energy gain by the electron from the field is much more rapid than any energy losses via elastic collisions.

Considering the continuity of the current to be fundamental for describing the plasma within the discharge, this should be the basis for any attempts to model its steady state behavior. A computationally inexpensive kinetic 1D model due to Godyak (19) uses such an approach to attempt to model the spatial evolution of the EEDF in the presence of a longitudinal inhomogeneity. His model will now be reviewed in some detail including discussion of its derivation, implementation of its method, modification of some of its characteristics, and evaluation of its utility in determining space charge effects on the EEDF.

III. Analysis: Orifice on Axis

3.1 Overview

The survey of space charge structures given in the previous chapter shows the space charge region is not described by equilibrium conditions. The electrons are not in equilibrium with the space charge field near the orifice since the energy input by the local electric field is not balanced by collisional energy losses. This is contrasted to the homogeneous portion of the positive column far from the orifice where the local electric field and the electrons are in equilibrium. The space charge region may be described as a nonequilibrium nonlocal transition zone imposed by the plasma to ensure constant current is maintained through the discharge across the abrupt change in geometry introduced by the orifice.

Godyak (19) attempts to characterize this phenomenon through experimental observation and a nonlocal approximate solution to the inhomogeneous Boltzmann equation. In this chapter, his measurements will be presented and then his approximate solution to the Boltzmann equation will be developed.

3.2 Godyak's Measurements

The geometry of the discharge is repeated here in Figure 16.
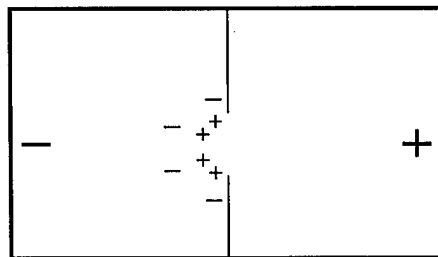
Figure 16   Geometry of discharge tube with orifice on axis and space charge sheath indicated. The large (-) and (+) symbols at either end represent the cathode and anode, respectively.

The discharge was composed of mercury vapor at low pressure (a few millitorr) and neon at 1 torr. The tube diameter was 5 cm and measurements were made for orifice diameters of 1.25 and 2.50 cm. His measurements of electric field, potential, electron number density (repeated from page 17), electron mean energy (repeated from page 17), and the EEDF (repeated from page 19) all measured on axis as a function of distance from the orifice are given in Figures 17,18,19.
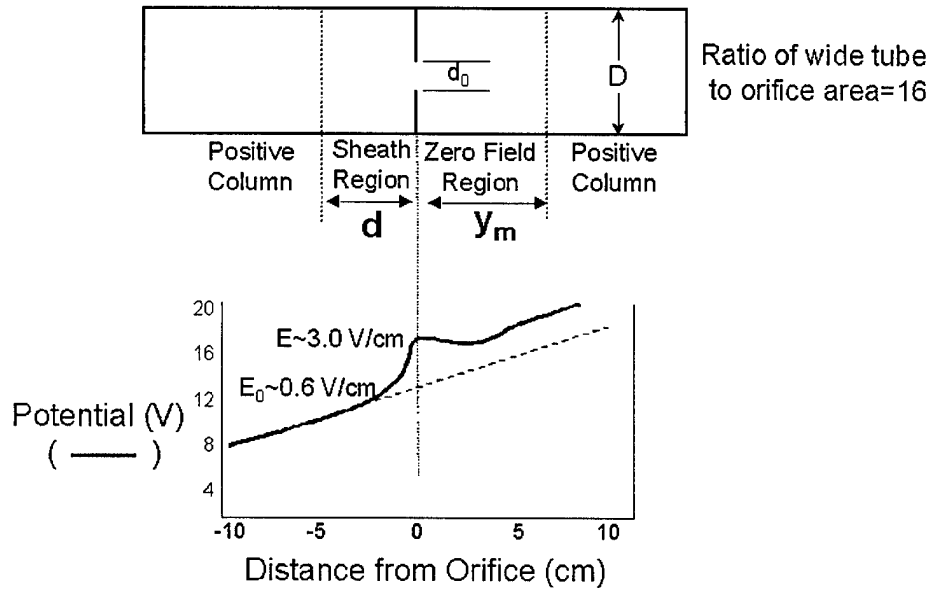
Figure 17   Axial electric field and potential measurements of Godyak (19) for orifice (diameter d_0=1.25 cm) on tube axis. Neon pressure=1 Torr, mercury pressure=6 mTorr, tube diameter=5 cm,current=0.2 A. Electric field values are at orifice and in homogeneous positive column (E_0), dashed line in plot indicates expected potential variation for homogeneous column with no orifice. d and y_m are the pre-orifice sheath length and the post orifice relaxation length respectively (Godyak (19)).

Beginning with Figure 17, the electric field in the pre-orifice region is shown to sharply increase near the orifice to a value about five times that of the field in the uniform positive column. Again, this is a consequence of the requirement for the current to be constant across the change in geometry caused by the orifice. The electron current density must be increased so that the current is constant across the decreased cross sectional area of the orifice. Past the orifice, this space charge

34
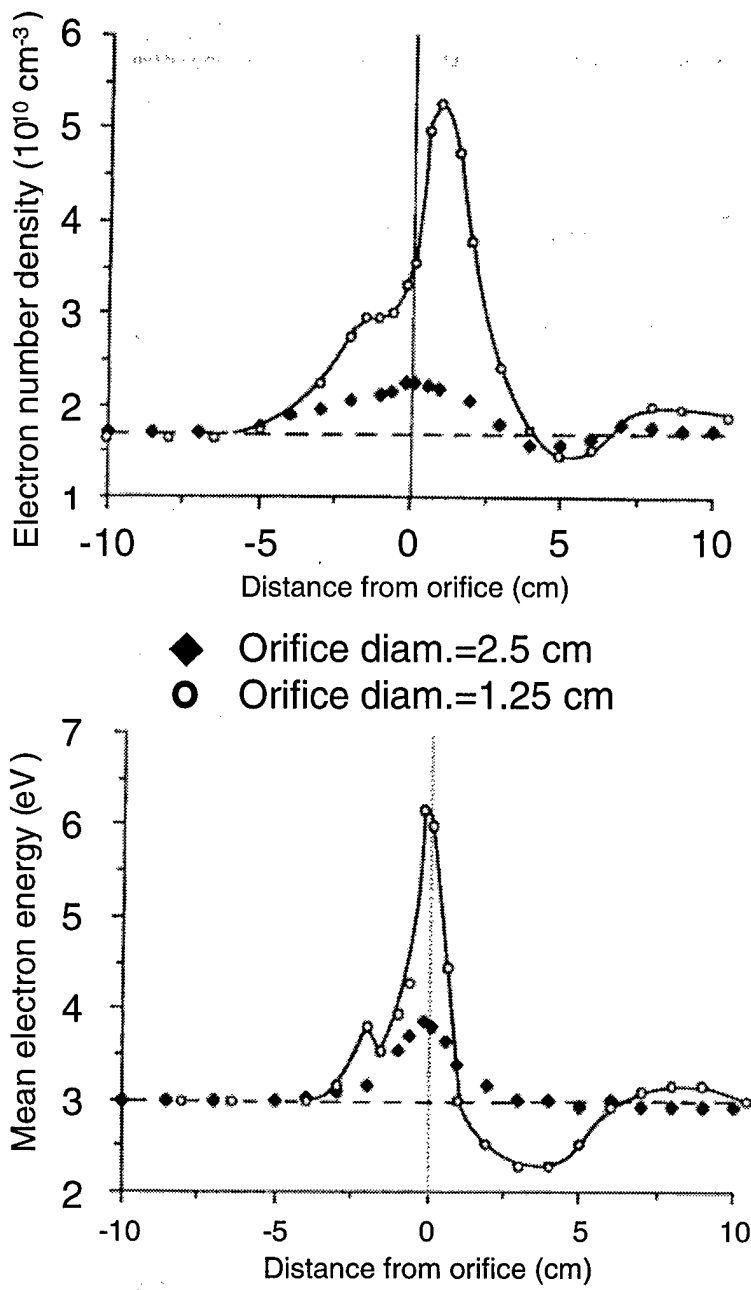
Figure 18   Measurements of axial variation of electron number density and mean energy for orifice on discharge axis, Hg-Ne pressure 1 Torr, current=0.1 A (after Godyak (19)).
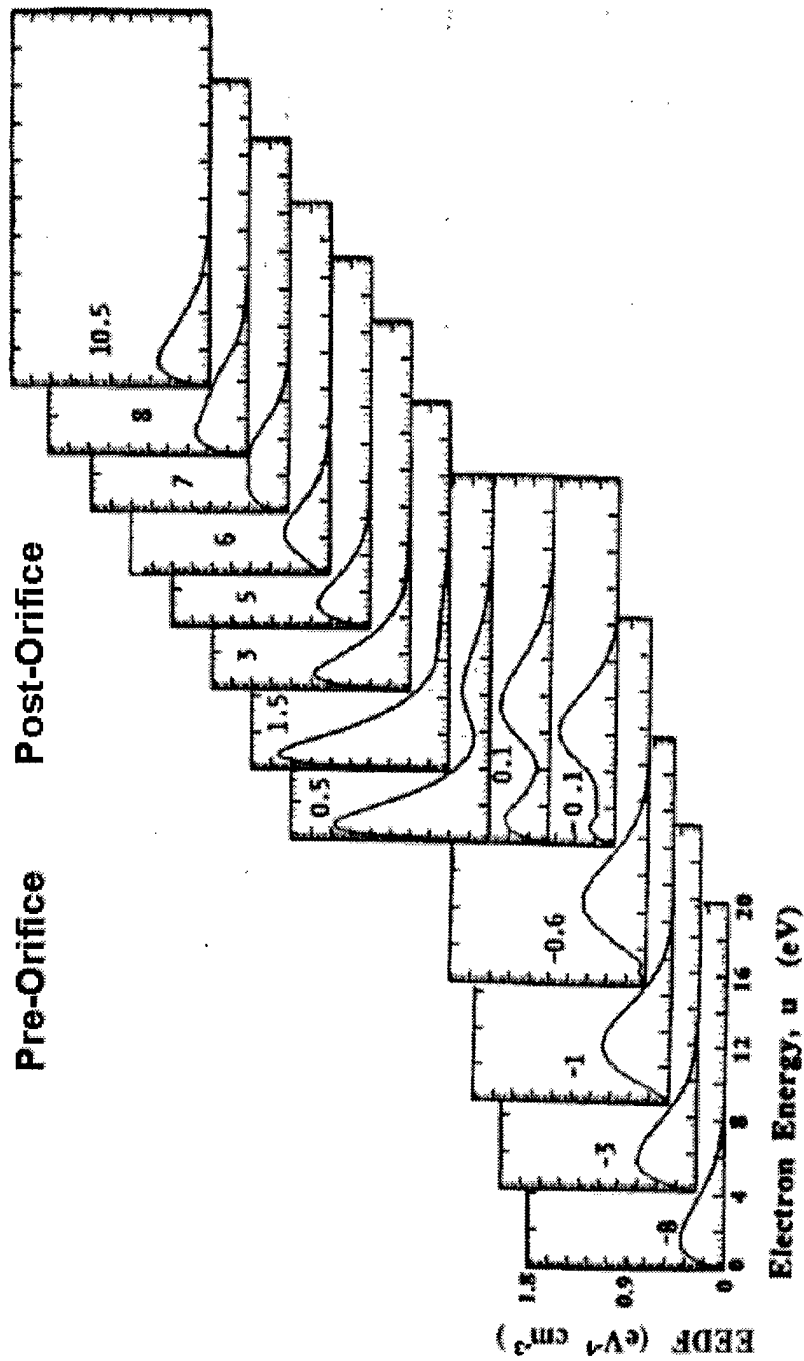
Figure 19   Spatial variation of axial EEDF from cathode to anode with orifice on discharge axis, Hg-Ne at 1 Torr, current=0.1 A. Note the numbers in the upper left of each panel indicate the distance from the orifice in cm, cathode side is pre-orifice, anode side is post-orifice, and the EEDF scale is divided by 10^9 (after Godyak (19)).

potential gradient is reversed such that it is an electron-decelerating field. This is a consequence of the gradient in electron pressure pointing toward the orifice as discussed in Chapter 2 for the constricted tube configuration. The associated space charge field on the anode side is directed oppositely to the discharge field. In general, the diffusion component of the field and the diffusion component of the electron current density dominate in the region where the axial gradients are present.

The plots in Figure 18 show the increased number density and mean energy of the electrons in the orifice region. As expected the larger the decrease in cross sectional area from the wide tube to the orifice, the larger the increase in the current density. For instance, the orifice diameter of 1.25 cm represents a decrease in cross sectional area by a factor of 16 compared to the wide tube cross sectional area so the product of the number density and drift velocity of the electrons must be increased by a factor of 16 to maintain current continuity. In this case, the result is an increase of just over 3 times for the number density and about 5 times for the drift velocity.

The axial variation of the centerline EEDF is given in Figure 19 where the number at the left of each panel indicates distance from the orifice. Here the nonlocal features are most evident. Following the distribution from the uniform positive column on the cathode side to the orifice reveals at first a gradual, then more drastic, migration of electrons to higher energies. Note that for this Hg-Ne mixture at the low mean energies realized, the mercury dominates the inelastic processes while the neon acts as a buffer gas mostly contributing only elastic collisions (the mercury inelastic threshold is about 5 Volts, approximately one third that of neon). Considering the amount of energy lost due to an elastic collision to be small since $\frac{m_e}{M} \ll 1$, the electrons accelerated through the sheath practically lose no energy until the inelastic threshold is reached. As the bulk of the distribution begins to reach the inelastic threshold energy, above-threshold electrons begin to scatter down to lower energies with a characteristic energy loss due to an inelastic collision being about 5 Volts in this case. This downscatter results in an increase of low energy electrons

37

on the side of the orifice adjacent to the anode. Here the plasma accommodates the requirement for constant current with a corresponding reversal in the space charge field and exhibits an excess of electrons due to the increased ionization in the region. Within about a centimeter of the orifice on the anode side, the increased density at lower energies causes elastic collisions as well as electron-electron interaction to dominate the electron kinetics. This is physically similar to the negative glow region near the cathode in terms of the electric field profile and dominant kinetic processes as discussed in Chapter 2.

The discussion of the measurements reveals the electron kinetics in the space charge region depend strongly on location. The sharp changes in electron drift velocity and density due to the inhomogeneity presented by the orifice cause the electron kinetics to have a nonlocal character. Energy gain and loss between the electric field and the electrons is not necessarily balanced in the space charge region. Energy gained by the electrons in the pre-orifice space charge enhanced field is not balanced by collisional losses. The electrons accumulate energy until inelastic processes begin to occur. Godyak attempted to develop a simplified kinetic model based on these nonlocal characteristics and his attempt will now be presented.

3.3 Godyak's 1-D Nonlocal Kinetic Approximation

3.3.1 Overview. Based on Godyak's measurements, the EEDF in the presence of an orifice on axis may be characterized as follows:

- Migration of electrons to higher energies and lower energies generally occurs in two different spatial regions

- The spatial dependence of the axial EEDF is a response to the perturbation of the axial space charge field

- Electrons practically conserve their total energy (kinetic+sheath potential) in the sheath region

These observations form a foundation for his model. Recalling the behavior of the electric field along the axis, he first adopts a one dimensional, stationary profile for the electric field as in Figure 20. The electric field is assumed constant in each region and zero in the post orifice region.
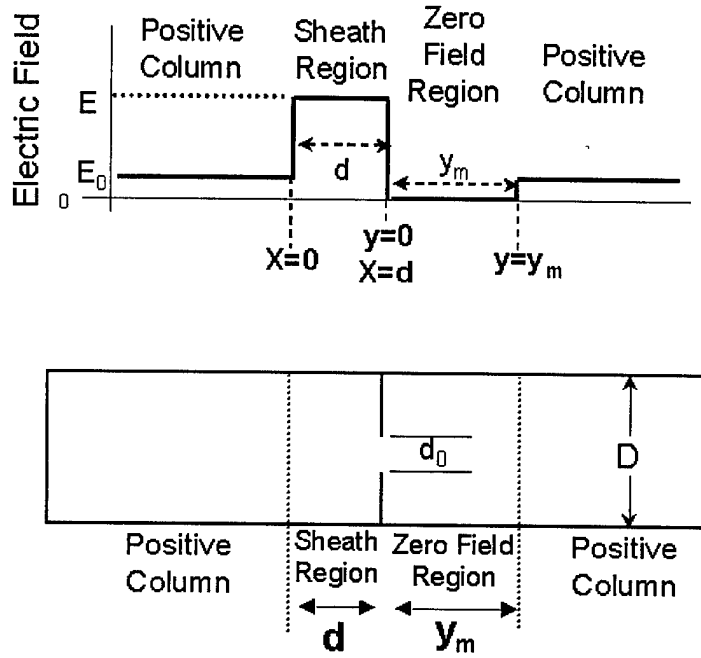
Figure 20   Coordinates and geometry for Godyak's nonlocal approximate solution to the one dimensional Boltzmann equation. E_0 is axial electric field in homogeneous column. x and y are both axial coordinates and differ only in choice of origin (x origin is boundary of sheath region, y origin is orifice) and $x = y + d$.

The distances d and y_m deserve mention. The distance d physically corresponds to the inelastic threshold energy acquisition length $\ell = u_1/E$ as discussed in Chapter 2 with u_1 the inelastic threshold energy and E the electric field. This is a somewhat intrinsic length in the plasma since the space charge field is determined by the degree of the inhomogeneity and this inelastic energy acquisition length is then determined by the inelastic threshold energy. The geometric boundary at the orifice marks the transition from energy gain to energy loss for the electrons where

that energy loss is due to the bulk of the distribution reaching the inelastic threshold energy. In his development, Godyak uses an approximation of 1.25 cm for this distance d based on his observation of the sheath. The distance y_m corresponds to the extent of the reduced field region and its role in the mathematical details of the development will be mentioned later. However, Godyak approximates this distance based on observation to be approximately 1.5 cm.

He further uses his measurements of the electric field as inputs to the kinetic equation. So, he uses his observations of the magnitude and extent of the space charge field and attempts to capture the response of the EEDF to space charge field inputs.

Other fundamental features of the development include:

- Steady state conditions

- Neglects momentum transfer energy losses, electron-electron interaction and sources

- Retains a single level inelastic collision model that accounts for excitation of mercury

His development will now be followed with enhancement and discussion where appropriate.

3.3.2 Development of Godyak's 1-D Kinetic Equation. The Boltzmann equation may be written as

$$\frac{\partial f}{\partial t} + \vec{v} \cdot \vec{\nabla}_{\vec{r}} f + \frac{\vec{F}}{m} \cdot \vec{\nabla}_{\vec{v}} f = (\frac{\partial f}{\partial t})_{coll} \tag{1}$$

where $f = f[\vec{r}, \vec{v}, t]$, $\vec{F}$ represents all applied forces, $(\frac{\partial f}{\partial t})_{coll}$ represents all collisional processes, and subscripted $\vec{r}$ and $\vec{v}$ indicate gradients taken in the configuration and velocity spaces, respectively. An approximate solution may be developed using

40

the first two terms of a Legendere expansion (the two-term approximation) of the distribution in velocity space as

$$f[\vec{r}, \vec{v}, t] = f_0[\vec{r}, v, t] + (\frac{\vec{v}}{v}) \cdot \vec{f_1}[\vec{r}, v, t] \tag{2}$$

with f_0 and f_1 representing the isotropic and anisotropic components of the distribution function assuming $f_0 \gg f_1$. The one dimensional model described here, with $f = f[v, x]$, allows representation of the resulting coupled equations, in steady state, as

$$\frac{v}{3}\frac{\partial}{\partial x}(f_1) - \frac{e}{3m_e}\frac{E}{v^2}\frac{\partial}{\partial v}(v^2 f_1) = Nq^*[v^*]\frac{v^{*2}}{v}f_0[v^*, x] - Nq^*[v]\,vf_0 \tag{3}$$

$$v\frac{\partial f_0}{\partial x} - \frac{e}{m_e}E\frac{\partial f_0}{\partial v} = -Nq_t v f_1 \tag{4}$$

with v the electron speed, E the axial electric field, N the neutral gas number density, q^* the total inelastic cross section , and $v^* = \sqrt{v^2 + \frac{2\,u_1}{m_e}}$, with u_1 the inelastic threshold energy and q_t the cross section for momentum transfer. These equations can be written in terms of the electron kinetic energy $u = m_e v^2/2e$ and specialized for the Hg-Ne gas mixture. The resulting coupled equations[1] for $f_0[u, x]$ and $f_1[u, x]$ are written as functions of the electron kinetic energy as

$$\frac{\partial}{\partial x}(\frac{uf_1}{3}) + \frac{\partial}{\partial u}(\frac{Euf_1}{3}) = N_{Hg}q^*[u + u_1](u + u_1)f_0[u + u_1, x] - N_{Hg}q^*[u]uf_0 \tag{5}$$

$$\frac{\partial f_0}{\partial x} + E\frac{\partial f_0}{\partial u} = -Nq_t[u]f_1 \tag{6}$$

Here f_0 is normalized such that

$$\int_0^\infty u^{1/2}f_0 du = n_e[x] \tag{7}$$

---

[1] The equations shown here reflect a correction of a misprint in Godyak's paper which is printed with an N in the denominators of the two derivative arguments on the LHS of the first equation.

41

where n_e is electron number density, u is the electron kinetic energy, E the axial electric field, N_{Hg} the mercury number density, u_1 the mercury excitation energy threshold, N the total gas number density, and q_t the neon cross section for momentum transfer. It should also be noted the f_0 and f_1 terms of equations (5), (6) are not the same f_0 and f_1 terms of equation (2). Additionally, the above equations ignore source terms (such as additional electron production due to ionization) energy losses due to momentum transfer, inelastic collisions with neon, and elastic collisions with mercury. Essentially, only the mercury atoms are excited and ionized with the neon serving as a buffer gas.

Introducing new independent variables

$$w = u, \quad \varepsilon = u - Ex \tag{8}$$

where w is numerically the kinetic energy but any differentiation or integration is performed at constant total energy ε, the sum of the kinetic and potential energies and E the electric field, a constant. The total energy variable ε is a consequence of the previous discussion regarding electron energy losses as small in the sheath region and captures the nonlocal aspect of the problem. With the new independent variables $[w, \varepsilon]$, derivatives with respect to $[u, x]$ may be represented as

$$\frac{\partial f[w, \varepsilon[u, x]]}{\partial u} = \frac{\partial f}{\partial w} + \frac{\partial f}{\partial \varepsilon}\frac{\partial \varepsilon}{\partial u} = \frac{\partial f}{\partial w} + \frac{\partial f}{\partial \varepsilon} \tag{9}$$

$$\frac{\partial f[w, \varepsilon[u, x]]}{\partial x} = \frac{\partial f}{\partial \varepsilon}\frac{\partial \varepsilon}{\partial x} = -E\frac{\partial f}{\partial \varepsilon}. \tag{10}$$

42

Noting now $f = f[w, \varepsilon]$ and substituting (8), (9), and (10) into (5), (6) yields[2]

$$-\frac{\partial}{\partial w}\left(\frac{w}{q_t[w]}\frac{\partial f_0}{\partial w}\right) = \frac{3NN_{Hg}}{E^2}\left((w+u_1)q^*[w+u_1]f_0[w+u_1, \varepsilon+u_1] - wq^*[w]f_0\right)$$

(11)

$$f_1 = -\frac{E}{Nq_t}\frac{\partial f_0}{\partial w}.$$

(12)

Note that the inelastic threshold energy for mercury is $u_1 \approx 4.7\ eV$, the inelastic cross section q^* is zero for energies below u_1. Godyak then uses the inelastic threshold energy to separate the problem into two energy domains

$$(i)\ w < u_1 \quad (ii)\ w \geq u_1$$

(13)

3.3.3 Pre-Orifice Solutions.

In front of the orifice, Godyak develops solutions in domain (ii) assuming

$$f_0[u+u_1, x] << f_0[u, x].$$

(14)

Accepting this restriction then the general solution may be obtained for the EEDF in each energy domain as

$$(w \geq u1) \quad f_0[w, \varepsilon] = C_2[\varepsilon]\phi[w]$$

(15)

$$(w < u1) \quad f_0[w, \varepsilon] = C_0[\varepsilon] - C_1[\varepsilon]\int_w^{u_1}\frac{q_t[\xi]}{\xi}d\xi$$

(16)

$$+C_2[\varepsilon+u_1]\int_w^{u_1}\tilde{I}[\xi+u_1]\frac{q_t[\xi]}{\xi}d\xi$$

---

[2]The differential equation for f_0 reflects a correction to a misprint in the original paper which omitted the leading (-) sign on the LHS.

where C_0, C_1, C_2 are arbitrary functions of the total energy and $\phi[w]$ is a particular solution of the above threshold, domain (ii), equation which is written as

$$\frac{\partial}{\partial w}\left(\frac{w}{q_t[w]}\frac{\partial f_0}{\partial w}\right) - \frac{3NN_{Hg}}{E^2}wq^*[w]f_0[w] = 0 \qquad (17)$$

This particular solution satisfies the boundary conditions $\phi[w] \to 0$ as $w \to \infty$ and $\phi[w] \to 1$ as $w \to u_1$. The third term on the RHS of (16) contains the collision term which may be expressed as

$$\tilde{I}[w] = \frac{3NN_{Hg}}{E^2}\int_{u1}^{w}\xi q^*[\xi]\phi[\xi]d\xi. \qquad (18)$$

This collision term may be simplified by using (17) and alternatively expressed as

$$\tilde{I}[w] = \frac{w}{q_t[w]}\phi^{'}[w] - \frac{u_1}{q_t[u_1]}\phi^{'}[u_1]. \qquad (19)$$

Thus, the general form for f_0 in front of the orifice is given by (15), (16), and (18).

3.3.3.1 Determination of Coefficients C_0, C_1, C_2.

The homogeneous region, where $E = E_0$, is described by the spatially uniform (homogeneous) solution which is characterized by $C_1[\varepsilon] = 0$ and $C_0 = C_2 = $ constant. The boundary condition at $x = 0$ marks the transition from the homogeneous region to the sheath region. With $C_1 = 0$, continuity of f_0 with respect to $[u, x]$ requires $C_0[\varepsilon] = C_2[\varepsilon]$. Further, the electron flux must be conserved at the boundary also. The electron flux density may be written with v_x as the x-directed (axial) velocity as

$$j = n_e[x]\bar{v}_x[x] \qquad (20)$$

where

$$\bar{v}_x[x] = \frac{\int v_x[x]f[v,x]d\vec{v}}{\int f[\vec{v},x]d\vec{v}}. \qquad (21)$$

Taking $u = m_e v_x^2/2e$ and the normalization condition from (7) leads to

$$n_e[x]\bar{v}_x[x] = \frac{E}{3N}\sqrt{\frac{2e}{m_e}} \int_0^\infty \frac{u}{q_t[u]} \frac{\partial f}{\partial u} du \qquad (22)$$

which may be evaluated using (16) for the below threshold, domain (i), contribution. The above threshold, domain (ii), contribution arises from (15), since $\frac{\partial f}{\partial w} = C_2 \phi'[w]$. The total electron flux density is the sum of these two contributions and is of the form

$$j = -\frac{E}{3N}\sqrt{\frac{2e}{m_e}} \left(\int_0^{u_1} C_1[\varepsilon]du - \int_0^{u_1} C_2[\varepsilon + u_1]\tilde{I}[u + u_1]du + \int_{u_1}^\infty \frac{u}{q_t[u]}\phi'[u]C_2[\varepsilon]du \right).$$
$$(23)$$

Since $C_2[\varepsilon]$ is an arbitrary function of the energy, it can be represented as a function of ε shifted by a constant as

$$C_2[\varepsilon] = \Phi[\varepsilon] + B_2. \qquad (24)$$

Recalling the restriction $f_0[u + u_1, x] << f_0[u, x]$, the third integral on the RHS of (23) may be truncated at $2\,u_1$ so that (23) becomes, after substituting the form for $C_2[\varepsilon]$ above,

$$j = -\frac{E}{3N}\sqrt{\frac{2e}{m_e}} \left(B_2\frac{u_1^2\phi'[u_1]}{q_t[u_1]} + \int_0^{u_1} C_1[\varepsilon]du + \frac{u_1}{q_t[u_1]}\phi'[u_1]\int_{u_1}^{2u_1} \Phi[\varepsilon]du \right). \qquad (25)$$

Since the flux is to be conserved, (25) must be independent of x. Thus, setting $\frac{\partial j}{\partial x} = 0 = -E\frac{\partial j}{\partial \varepsilon}$, the coefficient $C_1[\varepsilon]$ is determined

$$C_1[\varepsilon] = \frac{u_1\phi'[u_1]}{q_t[u_1]}\Phi[\varepsilon]. \qquad (26)$$

since

$$-\int_0^{u_1} \frac{\partial}{\partial \varepsilon} \left(C_1[\varepsilon] \right) \, du = \frac{u_1}{q_t[u_1]} \phi'[u_1] \int_{u_1}^{2u_1} \Phi[\varepsilon] du. \tag{27}$$

It can also be noted that by rearranging the limits of integration,

$$\int_{u_1}^{0} \frac{\partial}{\partial \varepsilon} \left(C_1[\varepsilon] \right) \, du \approx \int_{-u_1}^{-2u_1} \Phi[\varepsilon] du = \int_{u_1}^{2u_1} \Phi[\varepsilon] du. \tag{28}$$

if $\Phi[\varepsilon]$ is periodic with period= $2u_1$ such that for $\varepsilon < 0$, $\Phi[\varepsilon] = \Phi[\varepsilon + 2u_1]$. Now, equating the distribution of the electron flux density in the homogeneous region with that at $x = 0$ leads to

$$j_f[u] = -\frac{E}{3N} \sqrt{\frac{2e}{m_e}} \frac{u}{q_t[u]} \frac{\partial f_0[u,0]}{\partial w} \tag{29}$$

$$j_f[u] = \frac{E}{3N} \sqrt{\frac{2e}{m_e}} \frac{u}{q_t[u]} \psi[u]. \tag{30}$$

The above boundary condition yields $\Phi[\varepsilon]$:

$$(\varepsilon \geq u_1) \qquad \Phi[\varepsilon] = -\frac{\psi[\varepsilon]}{\phi'[\varepsilon]} - B_2 \tag{31}$$

$$(0 \leq \varepsilon < u_1) \quad \Phi[\varepsilon] = -\frac{q_t[u_1]}{u_1 \phi'[u_1]} \frac{\psi[\varepsilon + u_1]}{\phi'[\varepsilon + u_1]} \tilde{I}[\varepsilon + u_1] + \frac{\varepsilon}{q_t[\varepsilon]} \psi[\varepsilon]. \tag{32}$$

Godyak then claims f_0 will be continuous in ε if the two relations for $\Phi[\varepsilon]$ are related by

$$B_2 = -\frac{\psi[2u_1]}{\phi'[2u_1]} + \frac{2q_t[u_1]\psi[2u_1]}{q_t[2u_1]\phi'[u_1]} \tag{33}$$

however this is not strictly the case. When the two expressions for $\Phi[\varepsilon]$ in the appropriate domains are matched at u_1, the functions evaluate to the same value at

46

that point, but there is a discontinuity because

$$\underset{\varepsilon \to u_1}{Lim} \Phi_i[\varepsilon] \neq \underset{\varepsilon \to u_1}{Lim} \Phi_{ii}[\varepsilon] \tag{34}$$

where the subscripts i and ii denote the below and above threshold solutions, respectively. This discontinuity in the energy domain is not readily apparent[3] if $f_0[u + u_1, x] << f_0[u, x]$ is well satisfied, so it is presented here as a clarification. The truncation of the integration in (23) at $2 u_1$ is based upon $f_0[2u_1, x]$ being small in comparison to $f_0[u_1, x]$. The error introduced by the truncation of the integral is a discontinuity in the energy domain at $\varepsilon = 0$ because Φ was taken to be periodic for $\varepsilon < 0$. That is, $\Phi_i[\varepsilon = 0] = 0$ but $\Phi_{ii}[\varepsilon = 0] = \Phi_{ii}[2u_1] = \delta \neq 0$, where δ is some small finite value associated with the truncated integration of 23.

Additionally, the functions $\psi[u]$ are determined from (30) since the homogeneous region is described by (15),(16) and (18) with $C_0 = C_2 =$ constant$= B_0$, $C_1[\varepsilon] = 0$, and $E = E_0$ which is the electric field in the homogeneous region. The function may be written

$$(u \geq u_1) \quad \psi[u] = -\frac{E_0}{E_1} B_0 \phi_0'[u] \tag{35}$$

$$(u < u_1) \quad \psi[u] = \frac{E_0}{E_1} \frac{q_t[u]}{u} B_0 \phi_0'[u] \tilde{I}_0[u + u_1] \tag{36}$$

where these functions are another source of the discontinuity in $\Phi[\varepsilon]$ and also relate as in (34).

3.3.4 Post-Orifice Solutions.

Before proceeding with the post-orifice solutions, a reminder of the coordinates chosen is given here in Figure 21.

As shown in Figure 21, the region beyond the orifice is treated as a zero field region so that $E = 0$ is applied to (5),(6). The solutions in the post-orifice region

---

[3]Continuity of the distribution in the energy domain for the pre-orifice region is claimed by Godyak (19) but this is not strictly the case.
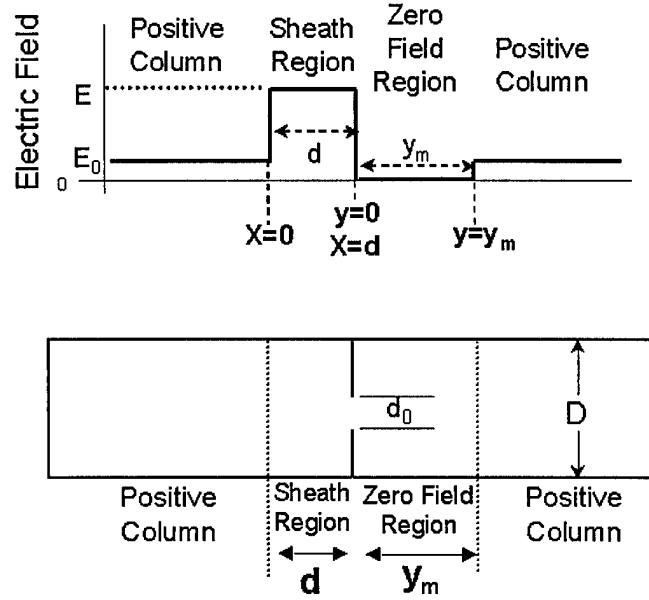
Figure 21   Coordinates and geometry chosen for Godyak's kinetic model.

then take the form

$$(u \geq u_1) \quad f_0[u,y] = A_2[u]Exp[-a[u]y] \tag{37}$$

$$(u < u_1) \quad f_0[u,y] = A_0[u] - A_1[u]y \tag{38}$$

$$+A_2[u+u1]F_q[u] \ (1 - Exp[-a[u+u_1]y])$$

where the functions A_0, A_1, A_2 are arbitrary functions of the kinetic energy, and

$$a[u] = \sqrt{3NN_{Hg}q^*[u]q_t[u]} \tag{39}$$

$$F_q[u] = \frac{q_t[u](u+u_1)}{q_t[u+u_1] \ u} \tag{40}$$

with the spatial variable y now indicating distance from the orifice. This solution in the post orifice region exhibits singular behavior as $u \rightarrow 0$, is discontinuous at $u = u_1$, and also is discontinuous in the spatial domain at the orifice where the transition from the pre- to post-orifice solutions takes place.

48

3.3.4.1 Determination of the Post-Orifice Coefficients. Determination of the coefficients beyond the orifice proceeds similarly to pre-orifice except in this region the electric field is set to zero, approximately matching observation. With $E = 0$, equation (6) takes the form

$$f_1[u, x] = -\frac{1}{N q_t} \frac{\partial f_0}{\partial x} \tag{41}$$

and the electron flux density is then

$$j = \frac{1}{3N} \sqrt{\frac{2e}{m_e}} \int_0^{u_1} \frac{u}{q_t[u]} A_1[u] du. \tag{42}$$

Note that j is not a function of x so that the conservation of the electron flux density is satisfied. The boundary condition for the distribution of the electron flux density, as in (30), is imposed at the orifice $(y = 0, x = d)$. So, the forms for the electron current density are matched at the orifice where the pre-orifice form is

$$j_f[u] = -\frac{E}{3N} \sqrt{\frac{2e}{m_e}} \frac{u}{q_t[u]} \frac{\partial f_0[u, x = d]}{\partial w} \tag{43}$$

and the post orifice form, using the distribution functions from (37), (38), (41) is

$$j_f[u] = -\frac{1}{3} \sqrt{\frac{2e}{m_e}} u f_1[u, y = 0]. \tag{44}$$

This results in

$$A_2[u] = -E \frac{\Phi[\varepsilon_d] + B_2}{a[u]} \phi'[u] \tag{45}$$

$$A_1[u] = -E \frac{u_1 \phi'[u_1]}{q_t[u_1]} (\Phi[\varepsilon_d] + \Phi[\varepsilon_d + u_1] + B_2) \frac{q_t[u]}{u} \tag{46}$$

where $\varepsilon_d = u - Ed$.

49

Note that the distribution function on this side of the orifice is not continuous at $u = u_1$ Godyak discusses this and notes that there is only downscatter occurring with the post-orifice solution. There is no mechanism for the reverse process since Coulomb interaction and the electric field in this region have been ignored. In addition, if the post-orifice distribution function is matched at the orifice to the pre-orifice distribution, the post-orifice solution rapidly becomes negatively valued due to the unrestricted downscatter. Godyak attempts to remedy this by forcing the below threshold form (38) at $y = 0$ to be at least as large as any possible decrease along the y coordinate in the space charge region. As mentioned earlier, Godyak uses the distance y_m to estimate the extent of the zero field region. As a result, A_0 is then determined to be

$$A_0[u] = A_1[u]y_m \tag{47}$$

where y_m is the length of the zero field region on the post-orifice side. Essentially, this is a non-physical remedy to the distribution and is a mathematical construct. Godyak treats the singularity at $u = 0$ by chopping the distribution function at a kinetic energy value estimated to be where electron-electron interaction would otherwise normally moderate the accumulation at lower energies. He sets the post-orifice distribution equal to a constant value, such that $f_0[u] = f_0[u_0]$ for $u < u_0$, where $u_0 \simeq (0.6 \times 10^{-12} n_e p_N y_m^2)^{6/7}$, with n_e in cm^{-3}, p_N neutral pressure in Torr, and y_m in centimeters.

3.4 Discussion

Before implementing Godyak's approximate solution to the Boltzmann equation, a review of some of the limitations of the development will be highlighted:

- The pre-orifice distribution function is not continuous in the energy domain at $\varepsilon = u_1$ and $\varepsilon = 0$. This can be alleviated, but not strictly removed, by ensuring $f_0[u + u_1, x] << f_0[u, x]$ is well satisfied.

- The post orifice distribution is discontinuous at $u = u_1$ and is singular at $u = 0$. This can not be remedied for this nonlocal approximation.

- The distributions are not continuous in the spatial domain across the orifice due to the simplified model of the electric field and the simplification of collisional processes.

These three limitations will be addressed below with some calculations of his approximate solutions. In addition, the results of his development will be evaluated for possible modifications addressing the limitations above and also for overall utility.

3.4.1 Implementation, Modification, Evaluation. Even with the above limitations, Godyak's approximate nonlocal solution to the one dimensional Boltzmann equation captures the effect of space charge on the EEDF qualitatively in the pre-orifice region. If qualitative agreement is achieved for the post-orifice region as well, it would seem fortuitous since relevant physical processes were omitted such as electron-electron interaction, elastic energy losses, and non-zero electric field. Some calculations and an interpretation of their utility will be presented here.

3.4.1.1 Pre-Orifice. Evaluation of the EEDF begins with equation (17). Imposing the boundary conditions as set forth earlier, it is easily solved numerically for $\phi[w]$. However, an analytic approximation was used instead so that a better understanding of the above threshold distribution, which is really the basis for the other solutions, could possibly be gained. This closes the equations to a completely analytic form. Initial attempts to parameterize the space charge effects on the EEDF for various reduced electric field (E/N) ratios is what helped lead to the initial realization that there were discontinuities in the solutions. The range of electric fields that can be input for typical gas pressures was limited to a few volts

per centimeter or else the discontinuities would become apparent. An analytic form for $\phi[w]$ is developed in the Appendix and repeated here as

$$\phi[w] = Exp[-\beta(w - u_1)]. \tag{48}$$

$$\beta^2 = \frac{3NN_{Hg}}{E^2}q^*q_t. \tag{49}$$

The corrected and modified theoretical development of Godyak was implemented using *Mathematica*.[®] The calculations were performed on a Pentium-class PC, with a complete determination of the distribution functions along with graphical displays executed in under 30 minutes.

The set of parameters used for the following results is for a mercury-neon discharge with neon pressure= 1 torr, mercury pressure= 1.2 millitorr, current= 0.1 A, $T_{Hg} = 40°C$. Godyak's values for the electric field $E_0 = 0.6$ V/cm and $E_1 = 2.8$ V/cm were measured for $T_{Hg} = 40°C$, with the sheath length (d) and zero field region length (y_m) approximated as 1.25 cm and 1.5 cm respectively. Plots of the homogeneous (spatially independent) EEDF, as well as the spatially dependent axial EEDF moving toward the orifice are given in Figure 22.

The top three panels depict the spatially dependent EEDF along the axis of the discharge; that is, they are plots of $u^{1/2} f_0[u, u - E_1 x]$ where $\varepsilon = u - E_1 x$. The lower panel provides a reference distribution in a tube of uniform radius (2.5 cm), representative of the form obtained far from the orifice. Discontinuities arise in the distribution functions, although Godyak claims the pre-orifice distributions are continuous. The lack of continuity of the solutions limits the parametric range for which the approach may be applied. As shown earlier in this chapter, there are two places where discontinuities may arise in the energy domain for the pre-orifice solution:

Moving toward Orifice

EEDF (eV⁻¹ m⁻³) EEDF (eV⁻¹ m⁻³) EEDF (eV⁻¹ m⁻³)

3×10^{15}
2×10^{15}
1×10^{15}

$2 \quad 4 \quad 6 \quad 8$
$u\ (eV)$

**Distance from
orifice = -1.0 cm**

1.25×10^{15}
7.5×10^{14}
2.5×10^{14}

$2 \quad 4 \quad 6 \quad 8$
$u\ (eV)$

**Distance from
orifice = -0.3 cm**

1.25×10^{15}
7.5×10^{14}
2.5×10^{14}

$2 \quad 4 \quad 6 \quad 8$
$u\ (eV)$

**Distance from
orifice = -0.1 cm**

EEDF (eV⁻¹ m⁻³)

1×10^{16}
8×10^{15}
6×10^{15}
4×10^{15}
2×10^{15}

$2 \quad 4 \quad 6 \quad 8$
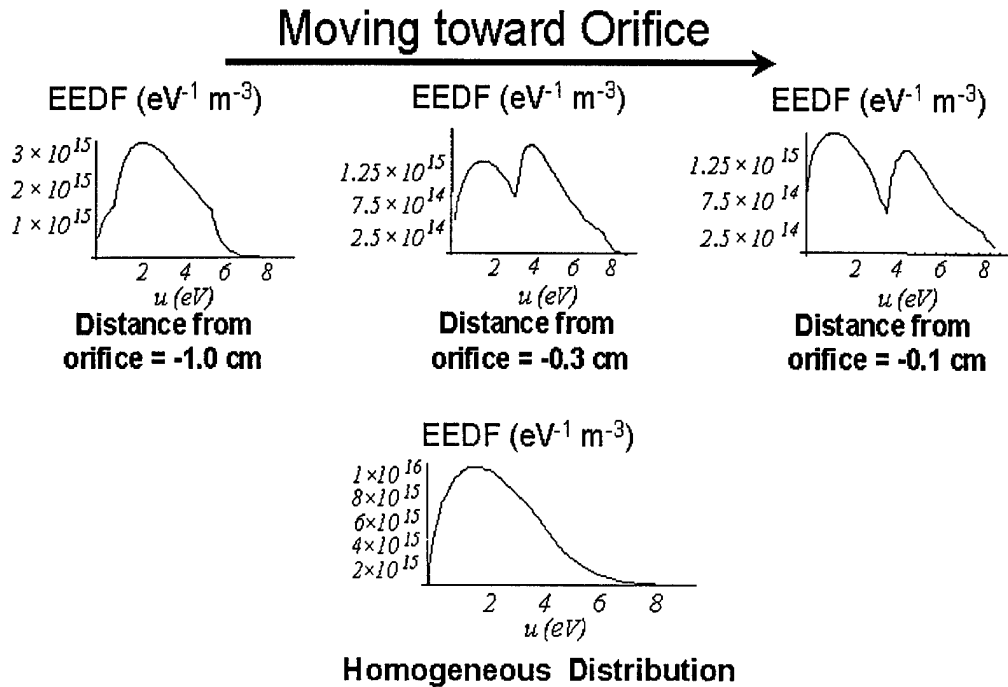$u\ (eV)$

Homogeneous Distribution

Figure 22   Calculations of the pre-orifice EEDF using Godyak's kinetic model for various distances from the orifice.

- $\varepsilon = u_1$

- $\varepsilon = 0$

The first, higher energy, discontinuity would occur for a distribution at a given x distance at a total energy $\varepsilon = u_1$. This would be at $u - E_1 x = u_1$, or along the kinetic energy axis at $u = E_1 x + u_1$. To illustrate, consider the top left panel of Figure 22. For the distribution plotted at an orifice distance of $y = -1.0$ cm, $x = 0.25$ cm (where $x = y + d$ with $y = 0$ the axial location of the orifice, x the distance from the start of the sheath, and $d = 1.25$ cm the sheath length), $u_1 = 4.7$ eV, and $E_1 = 2.8$ V/cm, the discontinuity occurs at 5.4 eV. In this plot of Figure 22, the distributions appear to be continuous but not necessarily smooth. However, the distribution is discontinuous and this may be shown most easily by plotting ψ from equations (35), (36) for a calculation at a slightly higher value of electric field as shown in Figure 23.

53

$$\psi \ (eV^{-5/2}cm^{-3})$$
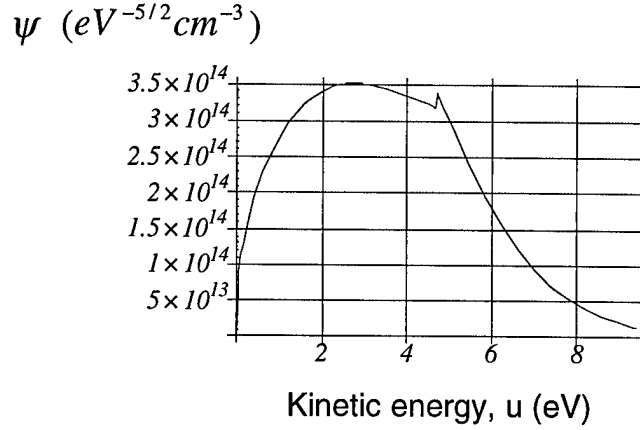

Kinetic energy, u (eV)

Figure 23   Plot of $\psi[u]$ with discontinuity at $u = u_1$.

The second discontinuity, $\varepsilon = 0$, will occur at a kinetic energy $u = Ex$. Referring again to the top left panel of Figure 22, $y = -1.0$ cm, $x = 0.25$ cm, $u_1 = 4.7$ eV, and $E_1 = 2.8$ V/cm, the discontinuity occurs at 0.7 eV. This would not appear to be a discontinuity if the restriction of $f_0[u + u_1, x] << f_0[u, x]$ is well satisfied. The location of this discontinuity is related to the truncation of the third integral in equation (23), but is still a manifestation of the functions (35), (36).

As a result, the comparison of calculations to observation is limited to qualitative aspects due to the discontinuity of the EEDF. However, the important physical processes are included in the pre-orifice region such as the electric field perturbation and an inelastically controlled collision regime. The calculated EEDFs seem to exaggerate the migration to higher energies and this is most likely due to the step-function form assumed for the electric field.

3.4.1.2   Collision Coefficients and Nonlocal Kinetics.   Once the distribution function is known, transport and kinetic parameters may be evaluated, e.g. mean energy, drift velocity, etc. Additionally, the total inelastic collision coefficient α^* and the ionization coefficient α_{ion} may be computed as

$$\alpha^*[x] = \sqrt{\frac{2e}{m_e}} N_{Hg} \int_{u_1}^{\infty} \frac{u}{j} q^*[u] f_0[u, x] \, du \tag{50}$$

54

$$\alpha_{ion}[x] = \sqrt{\frac{2e}{m_e}} N_{Hg} \int_{u_{ion}}^{\infty} \frac{u}{j} q_{ion}[u] f_0[u, x] \, du \qquad (51)$$

where these coefficients yield the average number of inelastic (or ionizing if α_{ion}) collisions per unit length of motion along the drift velocity direction. These collision coefficients, coupled with the space charge scale length, indicate the degree of non-locality of the kinetic environment. As Godyak points out, this may be illustrated by integrating the result over the length of the space charge structure through which the electron travels (19). For instance, to determine the probability an electron will experience an inelastic collision through a distance x, one may compute

$$P[x] = 1 - Exp[-\int_0^x \alpha^*[z] \, dz]. \qquad (52)$$

For this case, through the step region with $E = E_1 = 2.8$ V/cm, $P[d] = 0.49$, and so an average electron would have about an even chance to make it to the orifice with the accumulated energy from the space charge field for these inelastically controlled conditions. Results of calculations for mean energy $\bar{u}$, inelastic collision coefficient α^*, and ionization coefficient α_{ion} as a function of orifice distance are given in Figure 24.

3.4.1.3 Post-Orifice. Although a representative calculation will be shown for the post-orifice case, the determination of the distribution function is believed to be nonphysical and so should not be emphasized. A representative plot of the post orifice EEDF is given in Figure 25.

Godyak's nonlocal model gives reasonable qualitative agreement with his measurements in the pre-orifice region. However, the post-orifice distribution function is deemed to be unreliable and if qualitative agreement is achieved in any way, it
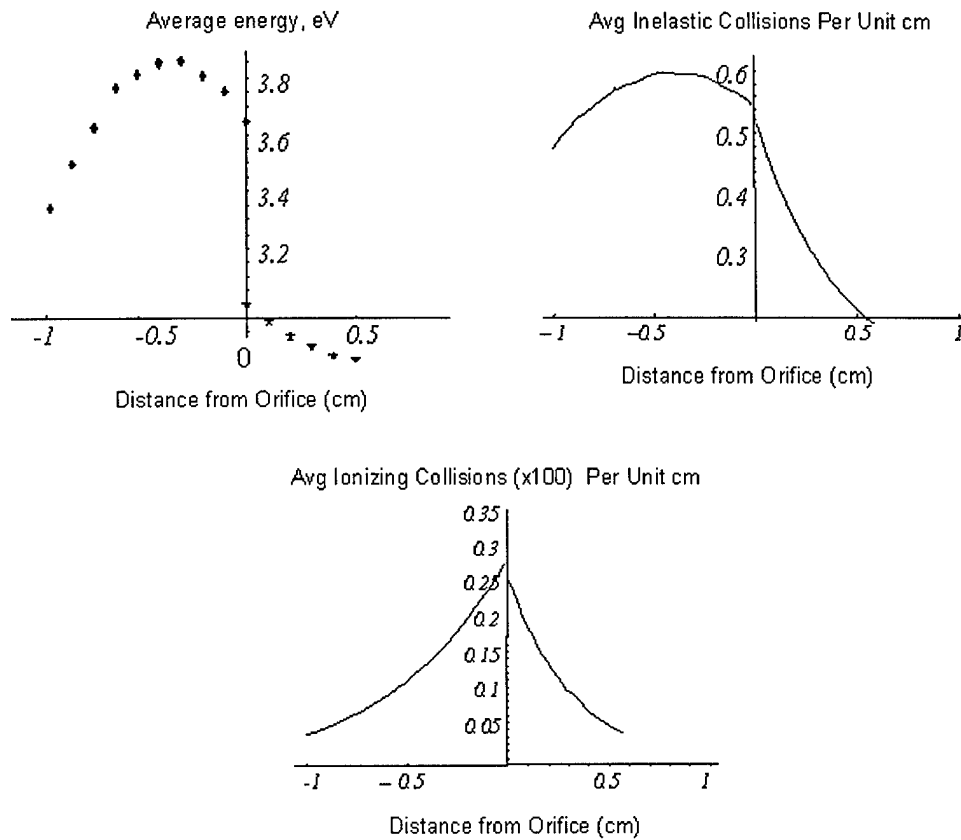
Figure 24   Calculation of average electron energy, inelastic collision coefficient, and
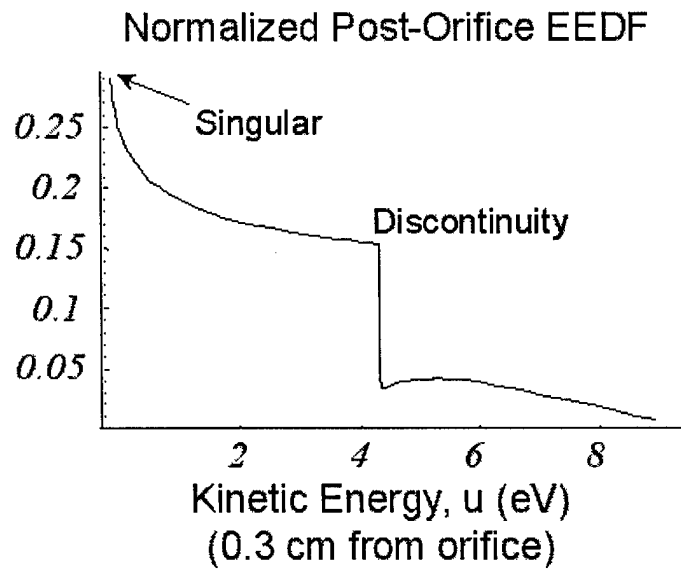ionization coefficient as a function of distance from the orifice.

Figure 25   Post-orifice calculation of normalized EEDF using Godyak's model.

seems fortuitous. Simply, there is no mechanism to migrate electrons to higher energies once they begin to accumulate in the below threshold energy regime. A discontinuity at $u = u_1$ reflects this lack of coupling. Neglect of various collisional processes such as electron-electron interaction and momentum transfer energy losses enforce this behavior. Thus, there are discontinuities in the energy domain associated with both the pre-orifice and post-orifice solutions. As a result of kinetic simplifications, the post-orifice solution is singular at $u = 0$. The distributions are also discontinuous in the spatial domain at the orifice. Godyak mentions most of the deficiencies associated with the post-orifice solution, but avoids direct mention of the limitations of the pre-orifice solution.

Godyak's nonlocal treatment does qualitatively reproduce the response of the EEDF upon approaching the orifice, is computationally simple to implement, and provides an understanding of nonlocal kinetics. It is, however, somewhat limited as to the magnitude and extent of the space charge it can model.

IV. Conclusions

The objective of this research was to survey the space charge structure arising from various inhomogeneities and characterize the nonlocal behavior of the electron energy distribution function (EEDF) due to an orifice on the axis of the discharge. The focus was to discuss, implement, modify, and evaluate an approximate nonlocal solution to the one dimensional Boltzmann equation after Godyak (19).

4.1 Survey of Space Charge Structures

All of the space charge structures surveyed involve nonequilibrium, nonlocal electron kinetics. A proper theoretical description requires a solution of the spatially inhomogeneous Boltzmann equation subject to the boundary condition of constant current.

For the stationary phenomena under consideration, a common physical interpretation emerges. Geometric inhomogeneities induce space charge structures that arise to maintain constant current through the discharge. Whether constricted or in the presence of an orifice, the plasma develops a space charge structure to link the uniform regions across the inhomogeneity.

The features of stationary inhomogeneities are present in the cathode sheath also: nonequilibrium, nonlocal electron kinetics. Although, the magnitude of the space charge in this region is much larger. The phenomenon here is related to the boundary condition imposed by the cathode for a much larger degree of inhomogeneity, but still similar in terms of energy gain and deposition when the cathode dark space and negative glow are compared to the pre-orifice and post orifice regions, respectively.

The electric field of these space charge regions may be viewed as a perturbation upon the quiescent plasma. It is, however, coupled to the plasma response and so while it affects the discharge, the discharge may also have a feedback influence.

This is indicative of nonstationary conditions associated with ionization waves. The transition to oscillatory behavior in the positive column is not as physically remote from the steady DC positive column as it may first seem. Oscillations in the plasma are often present due to self excitation and may even undergo growth. The study of small amplitude ionization waves adheres to the same features of nonequilibrium and nonlocality as for the stationary inhomogeneities. Advantages of non-fluid treatments are apparent in this case and lead to effects not predicted by fluid models in the case of moving striations (29).

Space charge structure associated with the shockfront in a plasma was also surveyed. Although no microscopic (EEDF) measurements are available, or even possible, at this time. A nonlocal approach, following the characteristics of the other phenomena surveyed, seems to be necessary to correctly model the shockfront dynamics and its interaction with the surrounding plasma.

4.2   Analysis: Orifice on Axis

The discussion and presentation of Godyak's measurements of EEDF, electron number density, mean energy, potential and electric field confirmed that the space charge region near the orifice is a region characterized by nonlocal electron kinetics. The nonlocal aspect of the problem was the space charge field arising near the orifice as a result of the maintenance of constant current. In the pre-orifice region, the field is enhanced and is an electron-accelerating potential drop. In the post-orifice region, the field is reduced.

The nonlocal approximate solution to the Boltzmann equation developed by Godyak qualitatively captures the space charge effects on the pre-orifice EEDF. The method is limited to a narrow range of conditions that does not permit it to be used in a quantitative parametric study of space charge effects on the EEDF. The solutions exhibit discontinuities in the pre- and post-orifice regions and singular behavior in the post orifice region.

59

Discontinuities occur in the distribution functions for fundamentally different reasons on either side of the orifice. In the pre-orifice region, the effect is subtle and is only plainly noticeable when the reduced electric field , E/N_{Hg}, is larger than approximately $\frac{3\,V/cm}{10^{14}cm^{-3}} \sim 3 \times 10^{-14}$ V cm^2. These discontinuities are related to mathematical simplifications made to solve the equations including truncating the integration of the electron flux density at $2u_1$ and using a periodic form for the $\Phi[\varepsilon]$ function for $\varepsilon < 0$. However, with the dominant kinetic processes modeled, the model qualitatively captures the spatial dependence and nonlocality of the EEDF.

In the post-orifice region, a discontinuity and singularity arise due to physical shortcomings of the model. Even though the measurements of the EEDF may have indicated otherwise, the effects of electron-electron interaction and energy losses due to momentum transfer are not included. Neglect of these quantities, as well as the assumption of a zero electric field in the post orifice region, results in an unacceptable solution.

4.3 Recommendations

Any further study of space charge structures in the presence of longitudinal inhomogeneities should be done with the spatially dependent Boltzmann equation. A steady state approach should still be acceptable for a stationary space charge structure. Approaches considered should probably include:

- A better representation of the electric field, i.e., non-constant, preferably with axial and radial dependence, or possibly an axial dependence and constant radial dependence.

- A more detailed representation of collisional processes including at least momentum transfer energy losses and electron-electron interaction.

Appendix A. Approximate Analytic Form for Godyak's $\phi[w]$

The above threshold homogeneous distribution function is the basis for determination of the spatially dependent distribution functions. Godyak's equation (17) written in terms of $\phi[w]$ is

$$\frac{\partial}{\partial w}\left(\frac{w}{q_t[w]}\frac{\partial\phi[w]}{\partial w}\right) - \frac{3NN_{Hg}}{E^2}wq^*[w]\phi[w] = 0. \tag{53}$$

This equation can be solved numerically by applying boundary conditions $\underset{w\to u_1}{Lim}\phi[w] = 1$, $\underset{w\to\infty}{Lim}\phi[w] = 0$. Still, an approximate analytic method compares favorably in this case. Assuming a solution

$$\phi[w] = Exp[-\beta w] \tag{54}$$

then (53) becomes

$$\phi\left(\frac{\beta^2 w}{q_t} - \beta\frac{\partial}{\partial w}\left(\frac{w}{q_t}\right)\right) = \frac{3NN_{Hg}}{E^2}wq^*\phi. \tag{55}$$

Assuming $q_t \approx q_0 w^{1/3}$, then $\frac{\partial}{\partial w}\left(\frac{w}{q_t}\right)$ above becomes $\frac{2}{3}\frac{1}{q_t}$. Making that substitution yields for the LHS

$$\phi\left(\frac{\beta^2 w}{q_t} - \frac{2}{3}\frac{1}{q_t}\beta\right) = \phi\frac{\beta}{q_t}(\beta w - 2/3) \tag{56}$$

Assuming $\beta w \gg 2/3$, then (55) gives

$$\beta^2 = \frac{3NN_{Hg}}{E^2}q^*q_t \tag{57}$$

so that application of the boundary conditions described above leads to

$$\phi[w] = Exp[-\beta(w - u_1)]. \tag{58}$$

61

Comparison with the numerical solutions for the conditions of interest shows this approximation to be valid. A representative comparison of the approximate analytic form, ϕ (solid line), versus the numerical solution to equation (53), f_0 (dashed line), is given in Figure 26.
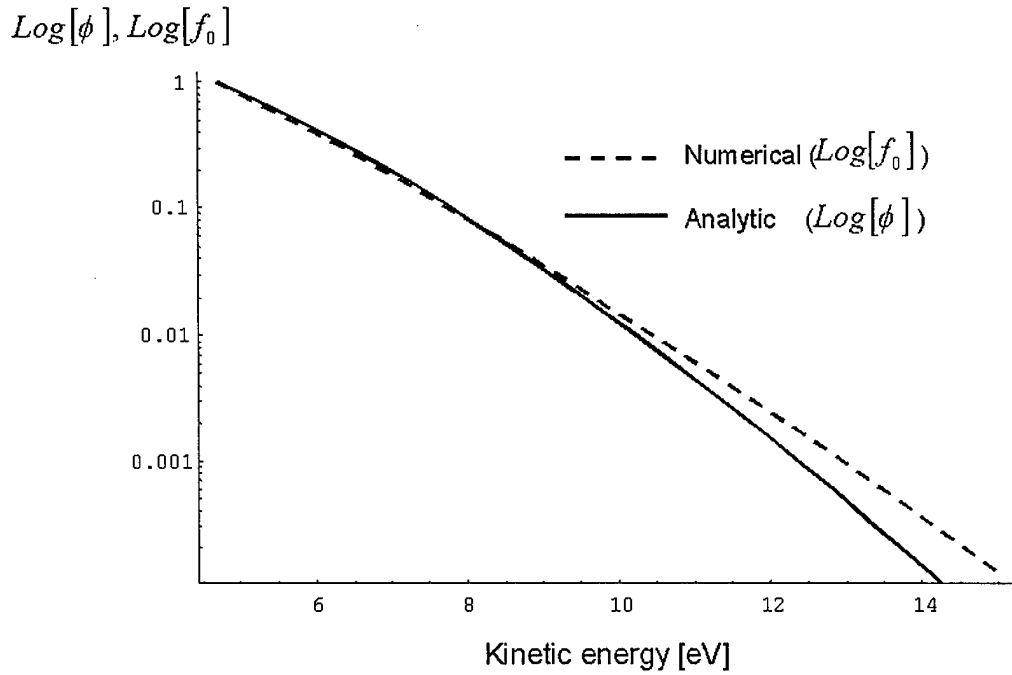

Figure 26   Approximate analytic solution ϕ and numerical solution f_0 to equation (53).

Bibliography

1. Adamovich, I.V., V.V. Subramaniam, and J.W. Rich "Phenomenological analysis of shock wave propagation in weakly ionized plasmas," AIAA 1998.

2. Andersson, D. "Measurements of electron energy distributions in front of and behind a stationary plasma sheath," J. Phys. D: Appl. Phys. 10:1549-1556 (1977).

3. Avramenko, R.F., A.A. Rukhadze, and S.F.Teselkin "Structure of a shock wave in a weakly ionized non-isothermal plasma," JETP Lett., 34(9):463-466(1981).

4. Baksht, F.G. and G.I. Mishin,. "Effects of vibrational relaxation on the parameters of shock waves in a molecular gas plasma," Sov. Phys. Tech. Phys., 28(5):547-549 (May 1983).

5. Barkhudarov, E.M., V.R. Berezovskii, M.O. Mdivnishvili, M. Taktakishvili, N.L. Tsintsadze, and T.Y. Chelidze "Dissipation of a weak shock wave in a laser spark in air," Sov. Tech. Phys. Lett., 10(10):498-499 (October 1984).

6. Basargin, I.V. and .G.I. Mishin, "Shock wave propagation in the plasma of a transverse glow discharge in argon," Sov. Tech. Phys. Lett., 11(2):85-87 (1985).

7. Basargin, I.V. and G.I. Mishin,. "Precursor of shock wave in glow-discharge plasma," Sov. Tech. Phys. Lett., 15(4):311-313 (1989).

8. Bennett, Eric, "Bolt–A Time-Dependent Boltzmann Solver." Unpublished, July 1996. Air Force Institute of Technology, Wright-Patterson AFB, OH.

9. Brown, S.C., *Introduction to Electrical Discharges in Gases*, Wiley and Sons (1966).

10. Buyanova, E.A., E.E. Lovetskii, and V.P. Silakov "Stationary shock waves in a nonequilibrium diatomic gas," Sov. J. Chem. Phys., 1(12):2856-2860 (1984).

11. Crawford, F.W. and I.L. Freeston. "The double sheath at a discharge constriction," Proc. 6th Int. Conf. on Phenomena of ionized gas, Paris, p. 461 (1963).

12. Levine, J.S. and F.W. Crawford. "Langmuir probe measurements of double layers in a pulsed discharge," J. Plasma Phys. (124):359-385 (1980).

13. Emeleus, K.G., "Tapered positive columns and plasma sacs," Int J. Electronics, 39(2):173-176 (1975).

14. Francis, Gordon. "The glow discharge at low pressure", *Encylopedia of Physics*, Vol. 22: Gas Discharges II, Springer-Verlag (1956).

15. Ganguly, B.N. and P. Bletzinger. "Shock wave dispersion in nonequilibrium plasma," Proc. of the AIAA conf. on hypersonic aircraft and space planes, Norfolk, AIAA 96:4607 (1996).

16. Ganguly, B.N. and P. Bletzinger. "Acoustic shock wave propagation in nonequilibrium nitrogen and argon," Proc. of the workshop on weakly ionized gases, USAF Academy, Colorado, (June 9-13 1987).

17. Ganguly, B.N.and P. Bletzinger "Shock wave damping and dispersion in nonequilibrium low pressure argon plasmas," Phys. Lett. A 230:218-220 (1997).

18. Garscadden, A. "Ionization waves in glow discharges", *Gaseous Electronics*, Volume I: Electrical Discharges, Academic Press (1978)

19. Godyak, V., R. Lagushenko, and J. Maya . "Spatial evolution of the electron energy distribution in the vicinity of a discharge tube constriction," Phys. Rev. A 38(4):2044-2055 (August 1988).

20. Gorshkov, V.A., A.I. Klimov, G.I. Mishin, A.B. Fedotov, and I.P. Yavor "Behavior of electron density in a weakly ionized nonequilibrium plasma with a propagating shockwave," Sov. Phys. Tech. Phys. 32(10):1138-1141 (October 1987).

21. Hilbun, William, "One-Dimensional Multi-Species and Two-Dimensional Single Fluid Euler Equations Solutions using the explicit MacCormack scheme." PhD Dissertation, Air Force Institute of Technology, Wright-Patterson AFB, OH, 1997.

22. Ingold, J., "Anatomy of the discharge", *Gaseous Electronics*, Volume I: Electrical Discharges, Academic Press (1978)

23. Jane's Defence Weekly, pp. 23-25, (June 17 1998).

24. Johnson, J.C., N. D'Angelo, and R. Merlino "A double layer induced ionization instability", Jnl of Physics D: Appl. Phys., Dec (1989)

25. Klimov, A.I., G.I. Mishin, A.B. Fedotov, and V.A. Shakhovatov "Shock wave propagation in a glow discharge," Sov. Tech. Phys. Lett., 8(4):192-194 (1982).

26. Klimov, A.I. and G.I. Mishin "Shock wave propagation in a decaying plasma," Sov. Tech. Phys. Lett., 8(5):240-241 (1982).

27. Klimov, A.I., A.N. Koblov, G.I. Mishin, and Y.L. Serov "Evolution of anomalous dynamic properties," Sov. Tech. Phys. Lett., 8(4):192-194 (1982).

28. Klimov, A.I., A.N. Koblov, G.I. Mishin, Y.L. Serov, K.V. Khodatev, and I.P. Yavor "Propagation of shock waves in a non-steady-state discharge," Sov. Tech. Phys. Lett., 15(10):800-802 (1989).

29. Kolobov, V.I., and V.A. Godyak "Nonlocal electron kinetics in collisional discharge plasmas", Transactions on Plasma Science, 23(4):503-531 (1995)

30. Mishin, G.I., A.I. Klimov, and A.Y. Gridin "Anomalous relaxation and instability of shock waves in gases," Sov. Tech. Phys. Lett., 26(11):1363-1368 (1981).

31. Montgomery, D.C. and D.A. Tidman, *Plasma Kinetic Theory*, McGraw-Hill (1964).

32. Ohe, K. and H. Yamada. "Distortion of plasma due to installation of a grid in homogeneous He positive columns," J. Phys. D: Appl. Phys. 27:756-764 (1994).

33. Papoular, R., *Electrical Phenomena in Gases*, Elsevier Publishing (1965).

34. Saeks, R. and E. Kunhardt. "Analysis of the electronic double layer effect in weakly ionized gas drag reduction," Proc. 2nd weakly ionized gases workshop, Norfolk, VA, AIAA (April 24-25 1998).

35. Sandahl, S., "Measurements of the ionization degree on the anode side of an electrical double sheath in a low pressure mercury discharge," Physica Scripta 3:275-278 (1971).

36. Sirghi, L., K. Ohe, and G. Popa "Interactions between ionization waves and potential structure formed at a constriction of the DC He positive column," J. Phys. D: Appl. Phys. 30:2431-2440 (1997).

37. Thomson, J.J. and G.P. Thomson, *Conduction of Electricity Through Gases*, Vol. II, Cambridge (1933).

38. Von Engel, A. *Ionized Gases*, Oxford,1965

Vita

Lieutenant Frank A. Tersigni ████████████████████

██

After working and attending college full time for about a year, Frank enlisted in the Air Force as an Air Traffic Controller and was an Honor Graduate from the Air Traffic Control Operator course in July 1990. Following an assignment at the Patrick Air Force Base Approach Control facility with the 45th Operations Support Squadron (AFSPACECOM), he attended Florida State University under the Airman Education and Commissioning Program (AECP, AFIT/CIRG). Frank completed a Bachelor of Science degree in Meteorology (Cum Laude) in April 1995, with subsequent commission as Second Lieutenant after completion of Officer Training School at Maxwell AFB in August of the same year. Frank's first commissioned tour of duty was with the 49th Fighter Wing (ACC) at Holloman AFB NM. While stationed at Holloman, Frank served as a mission weather briefer supporting the F-117A Stealth Fighter and completed the Basic Weather Officer Course at Keesler AFB as a Distinguished Graduate. In 1997, Frank entered AFIT to pursue his Master of Science degree in Physics with emphasis upon space environmental support. He was reassigned in March 1999 to the 21st Operations Support Squadron (AFSPACECOM) with duty at Peterson AFB, CO. ████████████████████

██

████████████████████████████

████████████████████

REPORT DOCUMENTATION PAGE			*Form Approved* *OMB No. 0704-0188*

1. AGENCY USE ONLY *(Leave blank)*	2. REPORT DATE March 1999	3. REPORT TYPE AND DATES COVERED

4. TITLE AND SUBTITLE
Space Charge Structure of a Glow Discharge in the Presence of a Longitudinal Inhomogeneity

5. FUNDING NUMBERS

6. AUTHOR(S)
FRANK A. TERSIGNI, 1st Lt, USAF

7. PERFORMING ORGANIZATION NAME(S) AND ADDRESS(ES)
AFIT/ENP
2950 P Street
Wright Patterson AFB, OH 45433
Advisor: William F. Bailey, COMM: (937) 255-3636 ext 4501
Email: william.bailey@afit.af.mil

8. PERFORMING ORGANIZATION REPORT NUMBER

AFIT/GAP/ENP/99M-14

9. SPONSORING/MONITORING AGENCY NAME(S) AND ADDRESS(ES)
AFRL/PR, Air Force Research Laboratory, Propulsion Directorate
Bldg 18
1950 Fifth Street
Wright Patterson AFB, OH 45433
Dr. Alan Garscadden COMM 937-255-2246

10. SPONSORING/MONITORING AGENCY REPORT NUMBER

11. SUPPLEMENTARY NOTES

12a. DISTRIBUTION AVAILABILITY STATEMENT
Approved for public release; distribution unlimited

12b. DISTRIBUTION CODE

13. ABSTRACT *(Maximum 200 words)*
A survey of space charge structures arising due to inhomogeneities in glow discharges was conducted. Space charge structures associated with tube geometries, the cathode sheath, striations, and shockwaves were examined. Space charge effects on the Electron Energy Distribution Function (EEDF) were explored for a geometric inhomogeneity using an approximate nonlocal solution to the one dimensional Boltzmann equation after Godyak. The approximate solution partially captured qualitative aspects of space charge effects on the EEDF. Simplification of collisional effects and adaptation of an approximate electric field restricted quantitative comparisons with experimental data. It is recommended that any future analysis of space charge effects on the EEDF should include energy losses due to elastic collisions, electron-electron collisions and a two dimensional representation of the electric field.

14. SUBJECT TERMS
Positive column, Electric double layer, Nonlocal electron kinetics, Boltzmann equation

15. NUMBER OF PAGES
77

16. PRICE CODE

17. SECURITY CLASSIFICATION OF REPORT	18. SECURITY CLASSIFICATION OF THIS PAGE	19. SECURITY CLASSIFICATION OF ABSTRACT	20. LIMITATION OF ABSTRACT
UNCLASSIFIED	UNCLASSIFIED	UNCLASSIFIED	UL